

A frequency stabilized diode laser system

Diploma thesis

provided by

Michael Sieghart

Matriculation number: 1701071

Bonn, March 2011

First examiner: Prof. Dr. Dieter Meschede

Second examiner: PD. Dr. Elisabeth Soergel

Contents

List of figures	V
1 Introduction	1
2 Properties of semiconductor lasers	2
2.1 Semiconductor lasers	2
2.2 Linewidth of a semiconductor laser	3
2.3 Injection locking	7
3 The fiber interferometer	9
4 Fabry-Perot cavities	12
4.1 Plane-parallel FABRY-PEROT cavities	12
4.2 Confocal FABRY-PEROT cavities	14
4.3 Coupling light into a cavity	16
5 Stabilization of the frequency	18
5.1 HÄNSCH-COULLAUD frequency stabilization scheme	18
5.2 Adapted HÄNSCH-COULLAUD scheme	21
6 Generating the setup	25
6.1 Diode laser	25
6.2 Building the cavity	27
6.3 Building the fiberinterferometer	29
6.4 The full setup	30
7 Results	36
8 Conclusion and outlook	39
A Appendix	41
A.1 Anti reflex coating	41

Bibliography	42
---------------------	-----------

Affirmation	45
--------------------	-----------

List of figures

2.1	Band model	2
2.2	Mode of a laser diode	3
2.3	Fluctuations of phase and amplitude due to spontaneous emission	4
2.4	Scheme injection locking	7
2.5	Competing frequencies during injection locking	8
3.1	Schematic setup of a self heterodyne fiber interferometer	9
4.1	Stability diagram of optical resonators	13
4.2	FABRY-PEROT-resonator	13
4.3	Confocal cavity used off axis	15
4.4	GAUSSIAN wave matching the cavity	16
5.1	Control loop	18
5.2	Frequency stabilization by HÄNSCH-COULLAUD	19
5.3	Capture range of the HÄNSCH-COULLAUD stabilization	21
5.4	Adapted HÄNSCH-COULLAUD stabilization setup	22
5.5	Cavity in V-configuration	22
5.6	Transmission of the adapted HÄNSCH-COULLAUD	23
6.1	LITTROW-configuration	25
6.2	PELTIER temperature control	26
6.3	Beam profile	26
6.4	Anamorphic pair of prisms	27
6.5	Threshold current	27
6.6	Parts of the cavity	28
6.7	Cavity with dimensions	28
6.8	CORNING [®] SMF TM -28 attenuation	29
6.9	The fiber interferometer	31
6.10	Optical isolator	32
6.11	Mount for the optical isolator	32

6.12	Observation part of the setup	33
6.13	Stabilization part of the setup	34
7.1	Measurement of the error signal	36
7.2	Measurement of the linewidth in LITTROW configuration	37
7.3	Measurement of the linewidth with feedback from the cavity	38
8.1	Fiber cavity	40
A.1	Properties of the anti reflex coating	41

1 Introduction

The motivation of this diploma thesis is to generate a *frequency stabilized diode laser system* which emits light at 852nm corresponding to the *D2* cesium transition to someday replace the locking laser for the cavity in the CQED experiment. Due to this the laser has to have a very narrow linewidth. In order to get such a system the laser will be locked to an external cavity i.e. the frequency fluctuations between the laser and the cavity must be reduced. It is required for the optical alignment to be such that light is returned into the laser only if the cavity is in resonance and reflected elsewhere when the light is off resonance. The original idea for such a system is based on the research results of HOLLBERG *et al.* in 1987 [3]. This diploma thesis aims to provide the reader with all necessary theoretical and practical knowledge in order to build such a system.

We will start by looking into the design and operating mode of semiconductor lasers. We will derive a formula describing their linewidth as well as discuss the dynamic properties of semiconductor lasers. This chapter will also explain what happens if we irradiate an external field into the laser cavity to investigate the possibilities for narrowing the linewidth of the laser and how to realize this. We have to study frequency selective components we want the laser to lock to and will explore how to build a servo loop to make the locking stable.

We will generate the servo loop by using a technique first proposed by HÄNSCH and COULIAUD in 1980. This technique is based on a polarization spectroscopy providing a dispersive error signal with a very broad capture range. To control our advance we have to find a method to measure the linewidth of the laser. This we will do with a self heterodyne scheme first proposed by OKOSHI *et al.* in 1985 which provides a high spectral breakup. Afterwards we will describe how the setup was generated, which problems have occurred and how they have been solved. At the end this diploma thesis will provide an outlook which steps can be taken to improve this experiment further on.

I want to thank Prof. Dr. DIETER MESCHEDE and his group for giving me the opportunity to compile my diploma thesis. Especially I want to thank WOLFGANG, TOBIAS and RENÉ for answering all my questions and JULIA for good collaboration and good mood in the lab. Furthermore, my thanks go to my wife BRITTA for giving me backup and confidence.

2 Properties of semiconductor lasers

The prediction of semiconductor lasers was already established 1953 theoretically by NEUMANN [14] and was realized in experiments little later. It took more than 20 years until semiconductor lasers got commercially successful products. Nowadays laser diodes are one of the most important optoelectronic components and cannot be count away from the work in labs and the daily routine. Therefore semiconductor lasers deserve an analysis of their structure and properties.

2.1 Semiconductor lasers

Semiconductor lasers or laser diodes are formed by a $p-n$ -junction and powered by injected electrical current. The physical origin of gain is illustrated in figure 2.1.

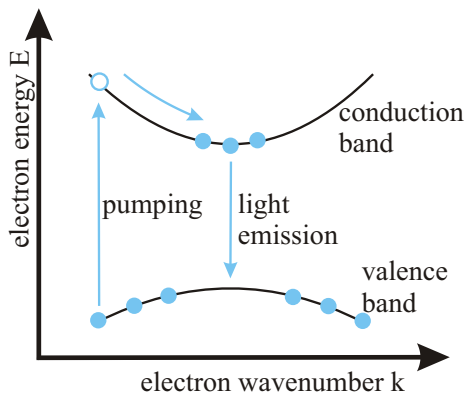


Figure 2.1: Model of the origin of gain in a semiconductor laser [30].

Normally most of the electrons are in the valence band. Electrical pumping excites electrons to a higher state in the conduction band. There they decay to states near the bottom of that band. Coincidental the holes generated in the valence band move to its top. Electrons in the conduction band then recombine with these holes, emitting photons near the energy of the band gap. This process is spontaneous, but can also be stimulated by incoming photons with adequate energy. A quantitative description is offered by the FERMI-DIRAC distributions for electrons in both bands. Electrical pumping with a direct current in forward direction of the laser diode ensures a continuous supply of electrons and holes. Population inversion has to be reached to generate coherent stimulated emission or lasing.

The current required to reach population inversion and starting the lasing process is called threshold current I_{th} .

The general internal structure of a laser diode and the synthesis of a laser mode is shown in figure 2.2. The occurring light wave leaves the semiconductor transverse to the driving current. It consists of a longitudinal and a transversal mode. The longitudinal mode shows

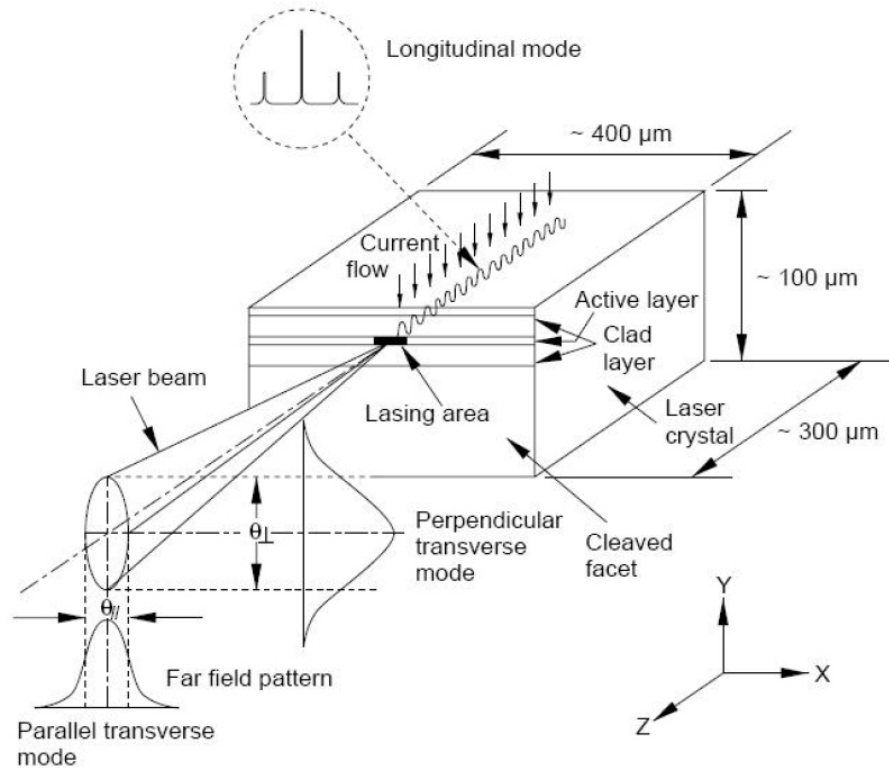


Figure 2.2: Structure and size of a laser diode. The laser mode leaves the semiconductor transverse to the driving current [27].

the position of the wave in z -direction. The position perpendicular to this mode is described by the transversal mode. The transversal mode is divided in a part perpendicular to the active layer and a parallel transverse mode. Because of the different components of the transversal mode in x - and y -direction, the emitted light has elliptical shape.

2.2 Linewidth of a semiconductor laser

Our task is to generate a diode laser system with a very narrow linewidth. In the following we will have a look into the theory of the linewidth of semiconductor lasers derived by HENRY [7] in order to understand why the linewidth is not small by nature. We will represent the field by β , which is a complex amplitude normalized in a way such that the average intensity

$I = \beta\beta^*$ also equals the average photon number in the laser cavity:

$$\beta = I^{\frac{1}{2}} \exp(i\phi).$$

Here $\phi(t)$ and $I(t)$ represent the phase and intensity of the laser field. We make the basic assumption that the n^{th} spontaneous emission changes β by $\Delta\beta_n$ having unit magnitude and random phase

$$\Delta\beta_n = \exp(i\phi + i\Theta_n) \quad \text{with } \Theta_n \text{ random.}$$

In other words, the linewidth of a laser can be seen as the result of fluctuations in phase of the optical field, caused by spontaneous emission events. These events effect the phase and intensity of the laser output, as illustrated in figure 2.3.

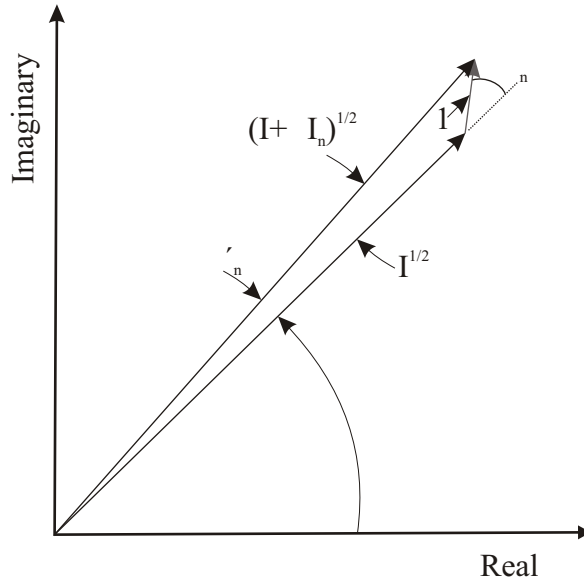


Figure 2.3: Changes of phase ϕ and intensity I of the field due to a single spontaneous emission n . The amplitude $\beta = I^{\frac{1}{2}} e^{i\phi}$ increases by $\Delta\beta_n$ with an amplitude of 1 and a phase $\phi + \Theta_n$, where Θ_n is a random angle [7].

Using this adoption of $\Delta\beta_n$ we can derive the rate equations to be [7]:

$$\dot{I} = (G - \gamma)I \quad \text{and} \quad \dot{\phi} = \frac{\alpha}{2}(G - \gamma). \quad (2.1)$$

Now we will solve these rate equations for changes in phase $\Delta\phi_n$ according to a single spontaneous emission event: A single spontaneous emission event changes I from steady state which leads to damped relaxation oscillations, returning I to steady state. Owing to the linearity of the equations describing small oscillations about the steady state, the total

change in phase for plenty spontaneous emissions coinciding in time is just the sum of the changes in phase ϕ_n .

Using figure 2.3 we can see that a change $\Delta\phi'_n$ occurs because of the out of phase component of $\Delta\beta_n$:

$$\Delta\phi'_n = I^{-\frac{1}{2}} \sin(\Theta_n)$$

There is a second contribution to the change in phase caused by the change in intensity. Looking at figure 2.3 and using the law of cosines we see that the amplitude is changed from $I^{\frac{1}{2}}$ to $(I + \Delta I_n)^{\frac{1}{2}}$ with

$$\Delta I_n = 1 + 2I^{\frac{1}{2}} \cos(\Theta_n). \quad (2.2)$$

The cosin term of (2.2) averages to zero. Therefore spontaneous emission in average causes a change of intensity according to adding one photon to the mode. Combining the two rate equations (2.1) we get

$$\dot{\phi} = \frac{\alpha}{2I} \dot{I}.$$

Initially we have $I(0) = I + \Delta I_n$ and after the relaxation $I(\infty) = I$. Therefore we will approximate I with the constant steady state value and find upon integrating

$$\Delta\phi''_n = -\frac{\alpha}{2I} \Delta I_n = -\frac{\alpha}{2I} \left(1 + 2I^{\frac{1}{2}} \cos(\Theta_n)\right). \quad (2.3)$$

So we get the total change in phase by (2.2) and (2.3):

$$\Delta\phi_n = \Delta\phi'_n + \Delta\phi''_n = -\frac{\alpha}{2I} + \frac{1}{I^{\frac{1}{2}}} [\sin(\Theta_n) - \alpha \cos(\Theta_n)] \quad (2.4)$$

Calling R the average rate of spontaneous emission, the first term of (2.4) is a small but constant phase change resulting in an average phase change

$$\langle \Delta\phi \rangle = -\frac{\alpha R t}{2I}.$$

The occurring total phase fluctuations for $N = Rt$ spontaneous emissions will be

$$\Delta\phi = \sum_{n=1}^N I^{-\frac{1}{2}} (\sin(\Theta_n) - \alpha \cos(\Theta_n)). \quad (2.5)$$

As a result of the spontaneous emissions, phase ϕ executes BROWNIAN motion which leads to a GAUSSIAN probability distribution [12]. It is readily shown [12] that

$$\langle \beta(t)^* \beta(0) \rangle = |\beta(0)|^2 e^{-\frac{|t|}{\tau_c}}$$

where $t_c = \frac{2t}{\langle \Delta\phi^2 \rangle}$. Here $\langle \Delta\phi^2 \rangle$ can be computed from (2.5) since the average of all cross terms vanishes for random angles:

$$\langle \Delta\phi^2 \rangle = \frac{R(1 + \alpha^2)t}{2I}.$$

It is shown [12] that the FOURIER-transform of the power spectrum of a semiconductor laser is $\langle \beta(t)^* \beta(0) \rangle$, which has a LORENTZian shape with a FWHM (**F**ull **w**idth at **h**alf **m**aximum) of

$$\Delta\nu = (\pi t_c)^{-1} = \frac{R}{4\pi I}(1 + \alpha^2). \quad (2.6)$$

In order to relate $\Delta\nu$ to the experiment we have to express I in terms of output power per facet P_0 , which leads to [7]:

$$I = \frac{2P_0}{h\nu v_g \alpha_m}.$$

Here $h\nu$ is the energy of the laser line, v_g the group velocity, r_m the facet reflectivity and $\alpha_m := -l^{-1} \ln(r_m)$ the facet loss, with l being the length of the cavity. According to [5] the rate of spontaneous emission R and the gain g are related by

$$R = v_g r = v_g a e^{\frac{eV - h\nu}{kT}} \quad (2.7)$$

$$G = v_g g = v_g a \left(e^{\frac{eV - h\nu}{kT}} - 1 \right) \quad (2.8)$$

with a being the optical absorption coefficient at the laser line and eV the separation of quasi FERMI-levels. Combining (2.7) and (2.8) we get

$$\frac{R}{v_g} = r = \frac{g}{1 - e^{-\frac{eV - h\nu}{kT}}} = a + g = g n_{sp} \quad (2.9)$$

where n_{sp} is the spontaneous emission factor. Combining (2.2),(2.6) and (2.9) we have

$$\Delta\nu = \frac{v_g^2 h\nu g n_{sp} \alpha_m (1 + \alpha^2)}{8\pi P_0} = \frac{2\pi h\nu (\Delta\nu_c)^2}{P_{out}} \cdot (1 + \alpha^2) = \Delta\nu_{ST} \cdot (1 + \alpha^2). \quad (2.10)$$

This formula gives the linewidth of a semiconductor laser with $\Delta\nu_c$ being the bandwidth of the laser resonator, P_{out} the output power of the laser and $\Delta\nu_{ST}$ the linewidth derived by SCHAWLOW and TOWNES in 1958 [20]. The linewidth formula (2.10) shows that the linewidth of a semiconductor laser has a bigger spread than e.g. a gas laser, caused by the greater bandwidth of the resonator of the semiconductor laser due to the very small length and the bad reflectivity of the laser cavity.

2.3 Injection locking

In the previous section we have seen that in normal laser operation, the noise of spontaneous emission is the seed for the amplification process resulting in coherent emission. Injecting an external signal into the resonator has a huge influence on this process.

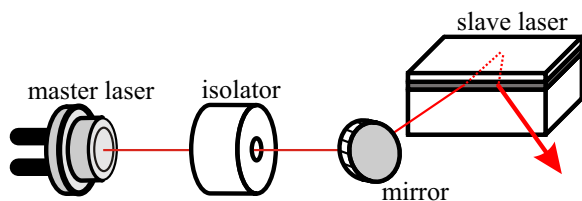


Figure 2.4: Basic setup for injection locking a diode laser. A stable signal from the master laser is injected in the slave laser and causes it to emit an amplified beam at exactly the same frequency [29].

Under certain conditions, which we want to discuss in the following the laser locks to the external signal. A basic configuration to achieve this is shown in figure 2.4, where a stable signal from a master laser is coupled into a slave laser.

Without any injected external signal, the laser is assumed to have a free running frequency of ω_0 with a maximum output intensity I_0 . It can be shown [21] that the injected frequency will have an intensity gain from input to output of

$$g_{int} = |g(\omega)|^2 \approx \frac{\gamma_e}{(\omega_1 - \omega_0)^2} \quad (2.11)$$

where γ_e is the energy decay rate of the laser cavity. Since the intensity is limited by saturation, injecting a weak external signal at a frequency $\omega_1 \neq \omega_0$ will start a competition for available gain. When ω_1 is brought closer to ω_0 , the gain available for the free running frequency will fall until it drops below threshold. Lasing at ω_0 will stop and all available power will be used to amplify the injected signal, which will run at an intensity equal to I_0 , possibly increased by the intensity of the injected light (figure 2.5). As soon as an equilibrium is reached, the laser continues emitting light exactly at the frequency of injection, as long as it stays in the locking range $\Delta\omega_{lock}$. The locking range is defined to be the area where the amplified output for the incident signal reaches I_0 . It is approximately given by [21]

$$\Delta\omega_{lock} \approx 2\gamma_e \frac{E_1}{E_0}. \quad (2.12)$$

Here $E_{0,1}$ are the amplitudes for the injected beam (index 1) and the emitted beam without any incident light (index 0). The most common way to describe the evolution of an injection

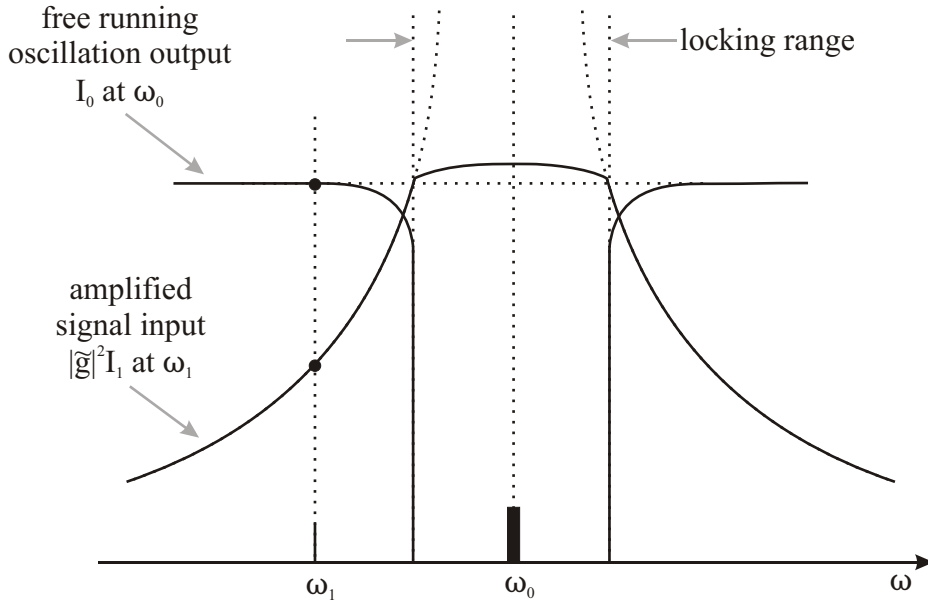


Figure 2.5: Free running oscillation competing with the injected signal as a function of the frequency offset between the free running frequency ω_0 and the injected beam with frequency ω_1 [21].

locked laser is the ADLER equation [21]:

$$\frac{d\phi(t)}{dt} + \omega_1 - \omega_0 = -\frac{\gamma_e E_1^2}{E_0^2} \sqrt{\frac{I_0}{I_1}} \sin(\phi(t)). \quad (2.13)$$

This equation has steady state solutions for the locking range and predicts the resulting oscillation to be running at the exact same frequency as the injected light in a steady state solution. This can be seen as a forced oscillator.

In fact stable lasers with narrow linewidth are not available at will. We can also build an *self injection locked* laser, where a part of the outgoing light is reflected back into the laser. By using frequency selective elements like FABRY-PEROT cavities we can affect the frequency the laser will lock to. The narrower the frequency we select, the narrower the laser frequency will be.

3 The fiber interferometer

The previous section explains what the linewidth of a semiconductor looks like as well as its spectral spread. For actually reducing the linewidth of the semiconductor laser we have to measure the actual linewidth of the laser to get the starting point as well as information about the progress in narrowing the linewidth. Therefore the next step is to have a look at methods to measure the linewidth of the laser.

There are plenty of possibilities such as conventional spectroscopy techniques like FABRY-PEROT interferometry. These techniques cannot dissolve very slow perturbations. Therefore we decide to concentrate our efforts on a method first proposed by OKOSHI et al., where a self heterodyne scheme provides a high spectral breakup [15].

In a self heterodyne setup the laser beam is splitted into two parts. One part passes through a single mode fiber to get a delay by time τ_d . The other part passes through an acousto-optic modulator to get a frequency shift of ν_s . Afterwards the throughputs of both paths are combined and get detected by a fast photo diode. A scheme of a so called *fiber interferometer* is shown in figure 3.1. In order to get a relation between the signal on the

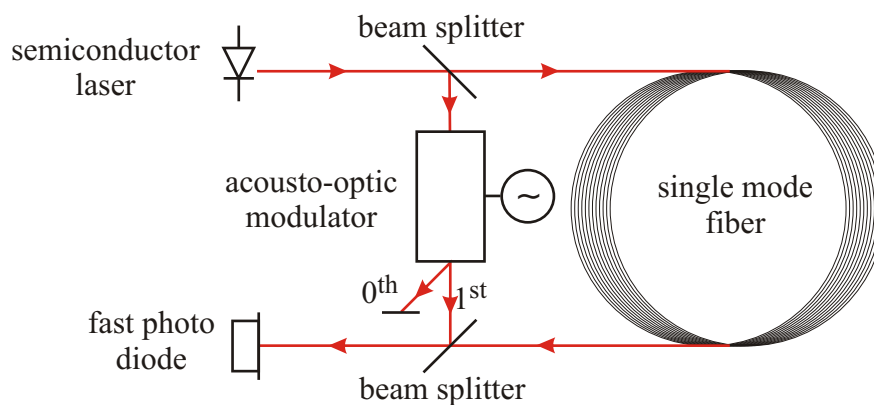


Figure 3.1: Schematic setup of a self heterodyne fiber interferometer.

photo diode and the linewidth we have to determine the reasons for the appearance of the signal.

The photo diode detects a superposition of two beams. One beam is delayed by time τ_d and the other beam is frequency shifted by ν_s . Therefore the total electrical field detected by the photo diode is

$$E(t) = E_0 \cdot [e^{i[(\omega_0 + \nu_s)t + \Theta(t)]} + e^{i[\omega_0(t + \tau_d) + \Theta(t + \tau_d)]}] .$$

Here ω_0 denotes the frequency of the laser and $\Theta(t)$ the phase noise at time t . The time delay is given by the length of the fiber L_{fiber} and its refractive index n_{fiber} as follows: $\tau_d = \frac{n_{\text{fiber}} \cdot L_{\text{fiber}}}{c}$. For time delays smaller than the time of coherence τ_c of the laser it is $\Theta(t + \tau_d) \approx \Theta(t)$ and the current of the detector $I_D(t) \propto E^*(t)E(t)$ cannot testify about the spectrum of the laser, which consists only of a constant peak in this case. Hence we have to concentrate our efforts on the case $\tau_c \ll \tau_d$ and have a look on the autocorrelation function. It is defined pertaining to the current of the detector I_D as follows [2]:

$$C_{I_D}(\tau) := \langle I_D(t) \cdot I_D(t + \tau_d) \rangle .$$

Here $\langle \dots \rangle$ denotes an average by time. With the assumption that the spontaneous emission is isotrop (which implies that $\Theta(t)$ has GAUSSIAN shape) and the definition of the changes of phase $\Delta\Theta(t, \tau) := \Theta(t + \tau) - \Theta(t)$ we can express the autocorrelation function as follows:

$$C_{I_D}(\tau) = S^2 E_0^4 \left[4 + 2e^{-2\frac{|\tau|}{\tau_c}} \cdot e^{\langle \Delta\Theta(t, \tau) \Delta\Theta(t + \tau_d, \tau) \rangle} \right] e^{i\Omega\tau} .$$

S is a proportionality factor between I_D and $|E|^2$. The WIENER-KHINTCHINE theorem states a connection between a spectral intensity distribution and the autocorrelation function via FOURIER-transformation [24]. This corresponds to the FOURIER-transform of the power spectrum and has LORENTZIAN shape. So we can express our spectra in case of long delay times $\tau_c \ll \tau_d$ as

$$S_{I_D}(\omega)_{\tau_d \ll \tau_c} = \frac{2S^2 E_0^4}{\pi} \left[4\pi\delta(\Omega - \omega) + \frac{\frac{4}{\tau_c}}{\frac{4}{\tau_c^2} + (\Omega - \omega)^2} \right] .$$

This spectra contains a DC -term and a LORENTZian distribution centered around the AOM-frequency Ω . The FWHM of this distribution is

$$(\Delta\omega)_{\text{FWHM}} = \frac{4}{\tau_c} = \frac{\mu}{\bar{n}t_c} = 2(\Delta\omega)_{\text{LASER}} . \quad (3.1)$$

$\mu = \frac{N_2}{N_2 - N_{1 \text{ thr}}}$ is the factor of population inversion, \bar{n} is the average number of photons in the laser mode and t_c is the durability of the photons in the laser resonator. The FWHM of the

spectral intensity distribution is proportional to the linewidth calculated in 2.10.

The resolution of this setup is given by the length of the fiber L_{fiber} and is

$$R = \frac{c}{n_{\text{fiber}}L_{\text{fiber}}} = \frac{1}{\tau_d} \quad (3.2)$$

at most. With this we know that our signal is LORENZian and the FWHM corresponds to twice the linewidth of the laser.

4 Fabry-Perot cavities

The linewidth of a semiconductor laser is strongly dependent on external feedback, as can be found in section 2.3. The narrower the linewidth of the external light the better the linewidth reduction of the laser itself. Since we want to lock to a FABRY-PEROT cavity we have to study its frequency selective properties to get a narrow feedback.

An optical resonator or cavity is an optical arrangement in which an incident light beam is mapped to itself multiple times. In a cavity with spherical mirrors the beams experience a periodic focusing action. This can be described mathematically as a periodic sequence of identical lens systems. A single element of the sequence is described by its ABCD matrix. The ray transfer of n consecutive elements of the sequence is characterized by the n^{th} power of that matrix. From this a stability criteria for optical resonators can be derived [10]:

$$0 \leq \underbrace{\left(1 - \frac{l}{R_1}\right)}_{=:g_1} \underbrace{\left(1 - \frac{l}{R_2}\right)}_{=:g_2} \geq 1 \quad (4.1)$$

A graphic representation of the stability criteria is shown in figure 4.1. The stable resonators lie in the grey regions. In the following we will have a look on two stable resonators, the *confocal* and the *plane-parallel*.

4.1 Plane-parallel Fabry-Perot cavities

A FABRY-PEROT-resonator consists of two parallel mirrors with high reflectivity (figure 4.2). In order to understand the transmission and reflection of the cavity dependent on the mirror spacing and the wavelength we look at the phase of the beams inside the cavity. To find the relative phase between a beam returning from a roundtrip and a beam just entering the cavity we keep the phase of the incoming beam constant and apply a phase propagation factor to the reflected beam [22]:

$$E_{1,(n+1)} = r_1 r_2 e^{2\pi i \frac{2l}{\lambda}} E_{1,(n)}. \quad (4.2)$$

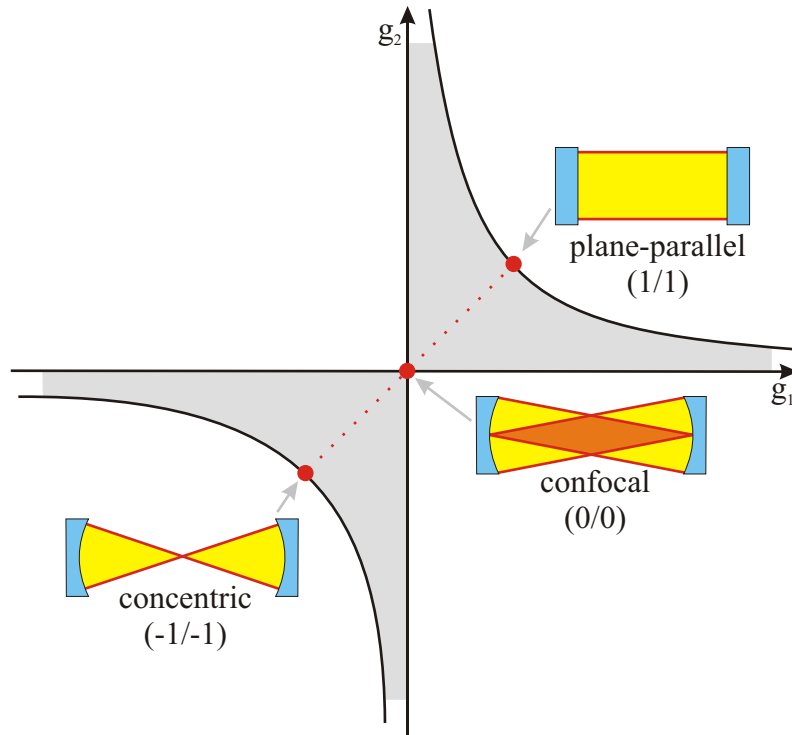


Figure 4.1: Stability diagram of optical resonators. Stable systems lie in the grey regions.

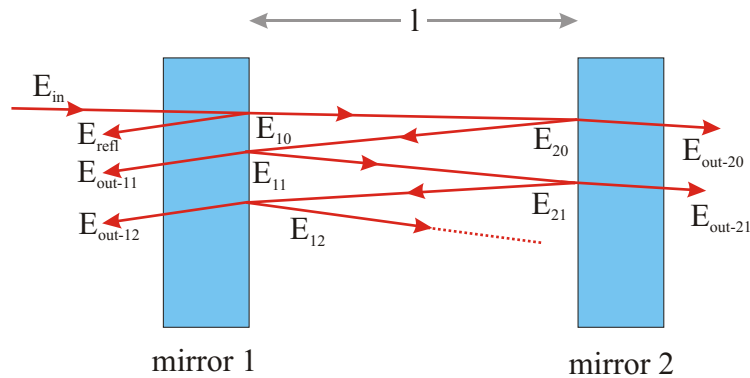


Figure 4.2: Light in a FABRY-PEROT-resonator consisting of two plan parallel mirrors. Drawn with non orthogonal incidence for clarity.

Here l is the mirror spacing, λ the wavelength of the light and $r_{1,2}$ the electric field reflectivities of the mirrors. Summing over all $E_{1(n)}$ we result in

$$E_1 = E_{int_1} \frac{1}{1 - (r_1 r_2 e^{2\pi i \frac{2l}{\lambda}})}. \quad (4.3)$$

Here $t_{1,2}$ denotes the electric field transmission of the mirrors. Now we can find the reflected and transmitted beams. For the transmitted beam we get

$$E_{out,2} = E_{in} \cdot \frac{t_1 t_2 e^{2\pi i \frac{2l}{\lambda}}}{1 - \left(r_1 r_2 e^{2\pi i \frac{2l}{\lambda}} \right)} \quad (4.4)$$

For the reflected beam we have to add the reflection of the incident beam to the beam having one round trip in the cavity:

$$E_{out,1} = E_{in}(-r_1)E_{in} \cdot \frac{t_1 t_2 e^{2\pi i \frac{2l}{\lambda}}}{1 - \left(r_1 r_2 e^{2\pi i \frac{2l}{\lambda}} \right)} \quad (4.5)$$

The reflectivity of the beam reflected back directly has to be $-r_1$ for being reflected at the other side of mirror 1.

For resonance, $\frac{2l}{\lambda}$ needs to be an integer. This corresponds to an equidistant set of resonant frequencies

$$\nu_{res} = n \frac{c}{2l}, \quad n \in \mathbb{N}. \quad (4.6)$$

The frequency spacing is defined as the free spectral range (FSR) of the resonator:

$$\Delta\nu_{FSR} = \frac{c}{2l}. \quad (4.7)$$

The linewidth of the resonant peaks can be found to be in good approximation [23]:

$$\Delta\nu_{FWHM} = \frac{c}{2l} \cdot \frac{1 - r_1 r_2}{\pi \sqrt{r_1 r_2}}. \quad (4.8)$$

The ratio of the free spectral range and the linewidth is defined to be the finesse \mathcal{F} :

$$\mathcal{F} = \frac{\Delta\nu_{FSR}}{\Delta\nu_{FWHM}} = \frac{\pi \sqrt{r_1 r_2}}{1 - r_1 r_2} = \frac{\pi \sqrt{R}}{1 - R}. \quad (4.9)$$

Here R denotes the reflectivity for the intensity.

4.2 Confocal Fabry-Perot cavities

In a confocal resonator with suitable mirror spacing even a beam that enters the cavity off axis will return to its point of entry after being reflected several times [21] (figure 4.3). In this off axis configuration a round trip consists of four passages through the cavity. Therefore

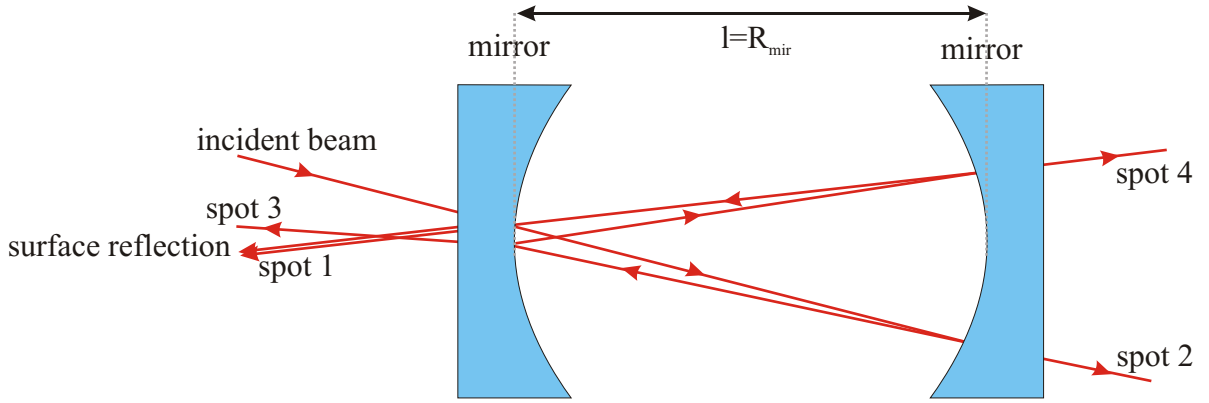


Figure 4.3: A confocal cavity used off axis. The incident beam has to be reflected several times to leave the cavity at the point of entry.

the free spectral range is $\Delta\nu_{FSR} = \frac{c}{4l}$. Using the picture of a round trip consisting of four reflections inside the cavity we can adapt the equations from a planar cavity: The amplitude $E_{out,2}$ of the first transmitted beam (spot 2 in figure 4.3) is similar to the transmitted beam of a planar cavity discussed above. The terms of the denominator of equation (4.3) correspond to the sum of contributions of all round trips. For the distance and number of reflections being doubled in comparison to the planar situation, $\frac{2l}{\lambda}$ in the phase propagation factor needs to be doubled also and the factor $r_1 \cdot r_2$ has to be squared. The enumerator describes amplitude and phase changes due to the transmission of the cavity and remains unchanged. This leads to the equation:

$$E_{out,2} = E_{in} \frac{t_1 t_2 e^{2\pi i \frac{l}{\lambda}}}{1 - (r_1^2 r_2^2 e^{2\pi i \frac{4l}{\lambda}})} \quad (4.10)$$

Adding the reflected beam of the entrance mirror to the beam that returns from inside the cavity we get the amplitude $E_{out,1}$ of spot 1 in figure 4.3. Hence the first part is unchanged, while the second part requires three reflections and four runs through the cavity until it leaves the resonator again. Considering the sum of all round trips in the cavity we get

$$E_{out,1} = -E_{in} r_1 + E_{in} \frac{t_1^2 r_1 r_2^2 e^{2\pi i \frac{4l}{\lambda}}}{1 - (r_1^2 r_2^2 e^{2\pi i \frac{4l}{\lambda}})}. \quad (4.11)$$

Since there are four possibilities leaving the cavity, the intensity in each individual spot is lower than for the parallel mirror setup.

4.3 Coupling light into a cavity

We need to discuss how to choose and align the optics for coupling light from the laser into the cavity. The optimization of this coupling requires consideration of two concepts [4]: *mode-matching* and *impedance-matching*. Mode-matching refers to the adjustment of the incoming beam to the cavity mode. Impedance-matching denotes the adjustment of the parameters of the cavity (e.g. mirror reflectivities). The coupling is maximized if the transmission through the input mirror is on par with all losses of the resonator. An example: A cavity consisting of two mirrors would be impedance-matched if the losses from the input mirror equals the sum of the losses of the second mirror plus the losses resulting from scatter and absorption on anything in the cavity including the mirrors. If this condition is fulfilled, the reflection of a spatially matched input beam will destructively interfere completely with the cavity wave transmitted back through the input mirror. Hence no net power will be reflected off the input mirror on resonance.

Matching the spatial mode of a laser beam to that of a confocal cavity needs some patience because the laser output is neither round nor diffraction limited. In general we have to transform a given beam into another beam with prescribed properties. The intensities of laser beams are not uniform. They are concentrated around the axis of propagation and their phase fronts are slightly curved. Therefore we have to match the curvature of the phase front to the curvature of the cavity mirrors (figure 4.4). To actually couple light into a cavity it is

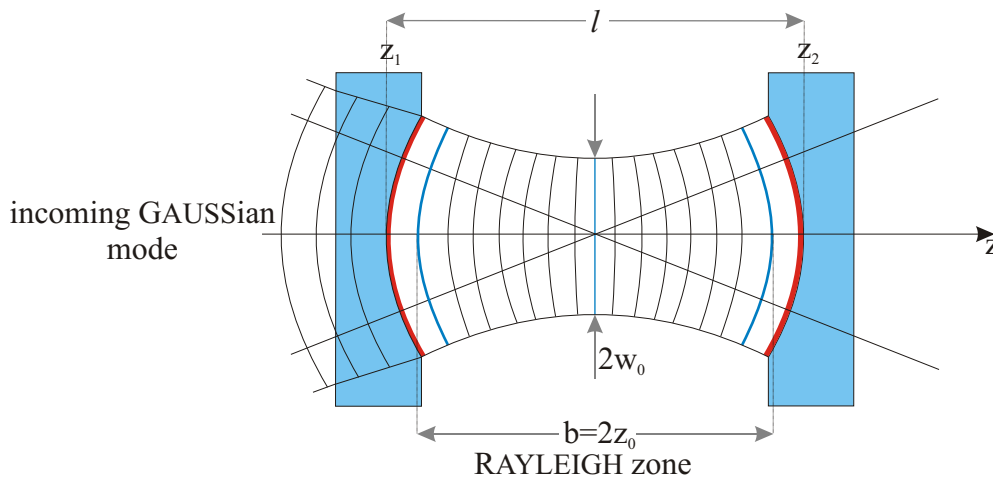


Figure 4.4: GAUSSIAN wave matching a cavity with curved mirrors. The curvature of the phase fronts have to match the curvature of the mirrors.

useful to think of a beam emanating from the cavity towards the laser. The waist and the

radius of curvature of this cavity beam can be calculated from the mirror geometry [10]. The task is to shape and focus the laser beam in a way that it approaches the conjugate of the cavity beam, i.e. generate a laser beam that is exactly like the cavity beam except moving towards the cavity.

To realize this it is reasonable to make sure that the laser beam is collimated and its cross section somewhat round. Afterwards at a fictitious point where the laser and the cavity beam are the same size, a planar convex lens of the proper power had to be placed to focus the laser beam to a waist at the same position as the waist of the cavity beam. If the collimated laser beam is larger than the cavity beam the beams cross sections have to be matched. Then the incoming laser mode matches the cavity mode.

5 Stabilization of the frequency

For stabilizing the frequency we need to generate an error signal which indicates the detuning of the laser compared to a reference frequency ω_{ref} . A controller has to compare the actual laser detuning from ω_{ref} and to adapt the frequency accordingly (figure 5.1). The

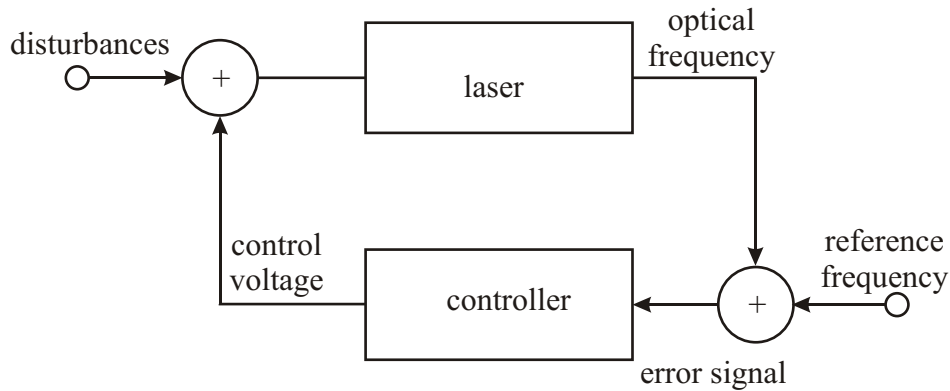


Figure 5.1: Control loop for stabilizing the frequency of the laser.

stabilization of the frequency is done in two parts: The first part is the stabilization against fast perturbations in the laser itself which is done via self injection locking as described in section 2.3. The second part is the stabilization for slow disruptions due to acoustic or thermal effects. This is done using a stabilization method first proposed in 1980 by HÄNSCH and COUILLAUD [8], providing a dispersive error signal without any need for modulation techniques.

5.1 Hänsch-Couillaud frequency stabilization scheme

Section 2.3 states that the output of a laser is strongly dependent on external feedback. We also have discussed frequency selection of a FABRY-PEROT cavity. Now we have to investigate the stabilization of the selected frequency against variations of the driving current of the laser, thermal differences and vibrations of the experimental setup.

We will use a method first proposed by HÄNSCH and COULLAUD [8] where a polarization spectroscopy is used in connection to an external cavity, to generate a signal similar to a dispersion signal. Basic principle is an element in the cavity which provides different losses for both orthogonal planes of polarization. This could be a glass plate at the BREWSTER-angle, a birefringent crystal or a polarizer. A schematic sketch of this setup is shown in figure 5.2.

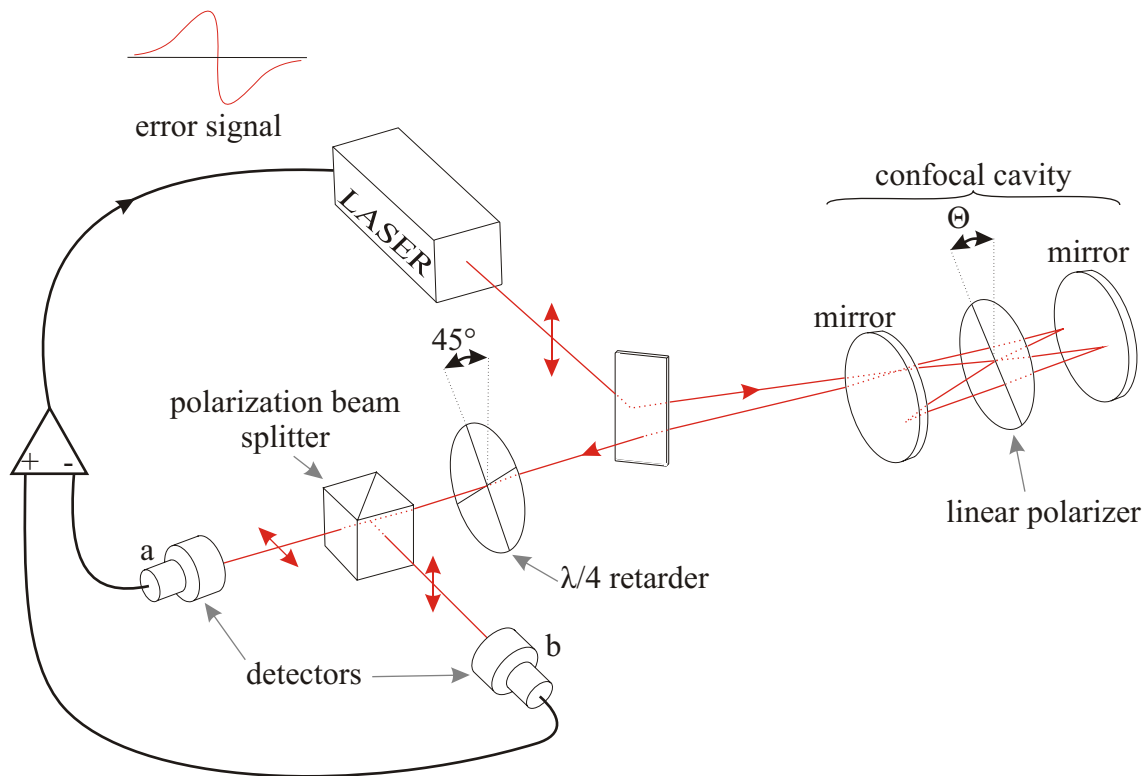


Figure 5.2: Setup for frequency stabilization by HÄNSCH-COULLAUD [8].

Let us have a look on the reflection of the light through the cavity [19]. If Θ is the angle between the direction of polarization of the incident light and the direction of polarization with minimal losses in the cavity we can write the incident light with amplitude E_0 in two components

$$\begin{aligned} E_{\parallel}^{(0)} &= E_0 \cdot \cos \Theta \\ E_{\perp}^{(0)} &= E_0 \cdot \sin \Theta, \end{aligned} \quad (5.1)$$

which are perpendicular and parallel respectively to the direction of polarization with minimal losses in the cavity. The complex amplitudes of the reflected wave add up to

$$E_{\perp}^{(r)} = E_{\perp}^{(0)} \cdot \sqrt{R_1}$$

$$\begin{aligned}
 E_{\parallel}^{(r)} &= E_{\parallel}^{(0)} \cdot \left(\sqrt{R_1} - \frac{T_1}{\sqrt{R_1}} \frac{R \cdot e^{-i\delta}}{1 - R \cdot e^{-i\delta}} \right) \\
 &= E_{\parallel}^{(0)} \cdot \left(\sqrt{R_1} - \frac{T_1 \cdot R}{\sqrt{R_1}} \cdot \frac{-R + \cos \delta + i \sin \delta}{(1 - R)^2 + 4R \sin^2 \frac{\delta}{2}} \right)
 \end{aligned} \tag{5.2}$$

where δ is a phase and R_1 and T_1 are the coefficients of reflectivity and transmission of the injection mirror. $R < 1$ is the factor of reduction of the amplitude taking all losses of one round trip into account or two round trips respectively if the laser is irradiated off axis. R accounts for any attenuation and determines the cavity finesse with equation (4.9). Both directions of polarization have different losses because of highly different finesse. So both directions of polarization get different phase shifts as long as the laser frequency does not match the resonance frequency of the cavity. At exact resonance ($\delta = 2n\pi$) both reflection coefficients are real which means that the reflected wave components remain in phase. Being off resonance $E_{\parallel}^{(r)}$ acquires a phase shift relative to $E_{\perp}^{(r)}$, owing to the imaginary part of $E_{\parallel}^{(r)}$. So the reflected beam is elliptically polarized which handedness is depending on the sign of detuning from resonance.

To detect the ellipticity, the reflected light is send through an analyzer ensemble. It consists of a $\frac{\lambda}{4}$ retarder, a linear polarization beam splitter and two photo detectors. The fast axis of the retarder is rotated by 45° relative to the polarization axis of the beam splitter output a (figure 5.2). This retarder transforms the incoming elliptically polarized light into two orthogonal linearly polarized waves. These linearly polarized waves are separated by a linear polarization beam splitter. The light intensities I_a and I_b are measured by two photo detectors connected to a differential amplifier.

If the incoming light is linearly polarized, the intensities $I_{a,b}$ are equal. The signal $I_a - I_b$ is only dependent on the magnitude and handedness of the ellipticity but not on a rotating angle of the analyzer assembly around the beam axis.

To calculate the signal we assume the assembly being rotated so that the fast axis of the retarder is parallel to the polarization axis of the intra cavity polarizer. We can find the field amplitudes measured by the detectors using the JONES calculus:

$$E_{a,b} = \frac{1}{2} \begin{pmatrix} 1 & \pm 1 \\ \pm 1 & 1 \end{pmatrix} \begin{pmatrix} 1 & 0 \\ 0 & i \end{pmatrix} \begin{pmatrix} E_{\parallel}^{(r)} \\ E_{\perp}^{(r)} \end{pmatrix}. \tag{5.3}$$

Hence the corresponding intensities on the detectors are

$$I_{a,b} = \frac{1}{2} c \varepsilon |E_{a,b}|^2 = \frac{1}{2} c \varepsilon \left| \frac{1}{2} \left(E_{\parallel}^{(r)} \pm i E_{\perp}^{(r)} \right) \right|^2. \tag{5.4}$$

Using equations (5.1), (5.2) and (5.4) we can calculate a signal

$$I_a - I_b = 2I^{(0)} \cos(\Theta) \sin(\Theta) \frac{T_1 R \sin(\delta)}{(1 - R)^2 4R \sin^2(\frac{\delta}{2})} \quad (5.5)$$

with $I^{(0)} = \frac{1}{2} c \varepsilon |E^{(0)}|^2$ being the intensity of the incident beam. The signal from (5.5) is plotted in figure 5.3. It is a combination of a steep resonant slope with far reaching wings.

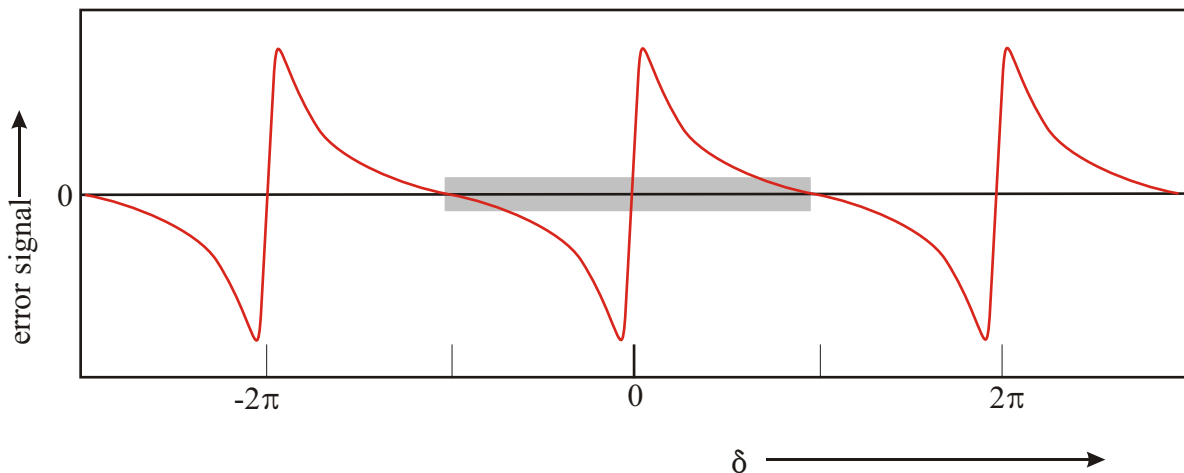


Figure 5.3: Error signal provided by the HÄNSCH-COULLAUD stabilization technique [19]. The grey region is the capture range.

This provides an ideal error signal for servo locking since it has a steep slope and a broad capturing range.

5.2 Adapted Hänsch-Couillaud scheme

The system described above has to be adapted to fit to the experiment. The original HÄNSCH-COULLAUD has no optical feedback for injection locking. So we adapted the system as shown in figure 5.4.

Here are two important differences to the original scheme: There is no polarizer in the cavity and we get feedback to the laser if the cavity is in resonance. This adoption is possible because the cavity is running off axis in V -configuration (figure 5.5). The type I beam is a superposition of the transmitted beam from the cavity and a reflected beam by the incident mirror. The type II beam is the transmission of the cavity. The entrance mirror of the cavity is coated with an anti reflex coating on the back of the mirror (appendix A.1) that the reflected elements of the type I beam are suppressed. So in a good approximation all

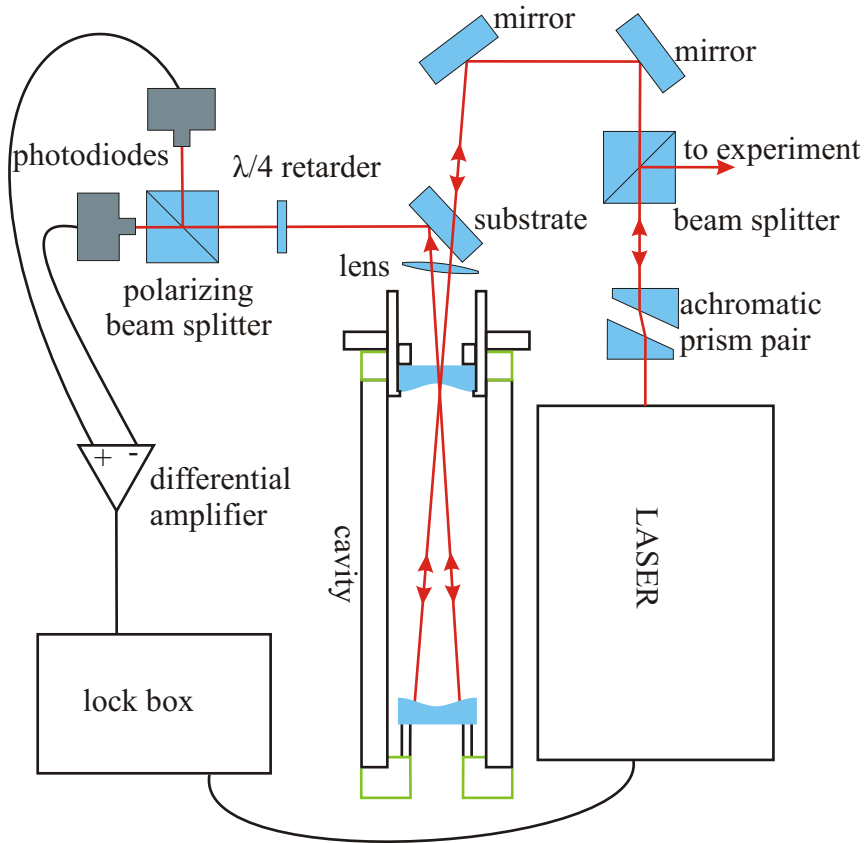


Figure 5.4: Adapted HÄNSCH-COULLAUD stabilization setup. A part of the transmitted beam of the cavity is send back into the laser.

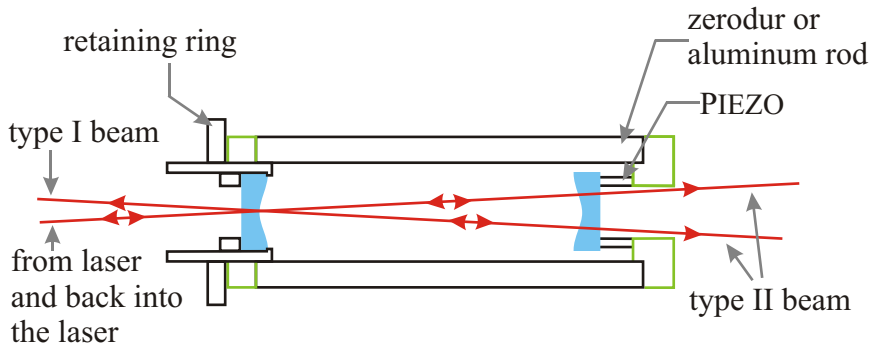


Figure 5.5: Cavity in V-configuration. Type *I* beam is a superposition of a reflected beam on the incident mirror and transmitted beam of the cavity. Type *II* beam is a transmitted beam.

beams leaving the cavity are transmission beams. In equation (4.10) we found the intensity

of the transmitted beam, but it also allows us to look at its phase.

$$E_{out,2} = E_{in} \frac{t_1 t_2 e^{2\pi i \frac{l}{\lambda}}}{1 - \left(r_1^2 r_2^2 e^{2\pi i \frac{4l}{\lambda}} \right)} \quad (5.6)$$

Comparing the transmitted beam to an imaginary reference beam, passing through the cavity without any reflections we get:

$$E_{rel} = \frac{E_{out,2}}{E_{ref}} = \frac{E_{out,2}}{t_1 t_2 e^{2\pi i \frac{l}{\lambda}}} = \frac{1}{1 - \left(f e^{2\pi i \frac{4l}{\lambda}} \right)} \quad (5.7)$$

Here we have introduced the roundtrip factor $f := r_1^2 r_2^2$. In resonance, all contributions from the electric field in the resonator have exactly the same phase. Therefore the transmitted light has exactly the same phase as that of the reference beam, meaning the relative phase to be zero independent of f . In the center between two resonances the phase difference between one round trip and the next are huge and cancel out each other, resulting in a net phase of zero again.

In the area close to a resonance the interesting part happens: Here only the circulating part gets a minimal phase shift between the round trips, and the amplitude drops to zero before canceling each other. For a high finesse cavity, many reflections will occur before the intensity goes close to zero. This leads to an increased contribution from the round trips having accumulated a larger phase shift. For an ultra low finesse cavity without mirrors there would be no phase shift for all wavelengths. Hence the slope of the phase around a resonance is strongly dependent on the round trip factor f and with it on the cavity finesse $\mathcal{F} \approx \frac{\pi\sqrt{f}}{2(1-f)}$.

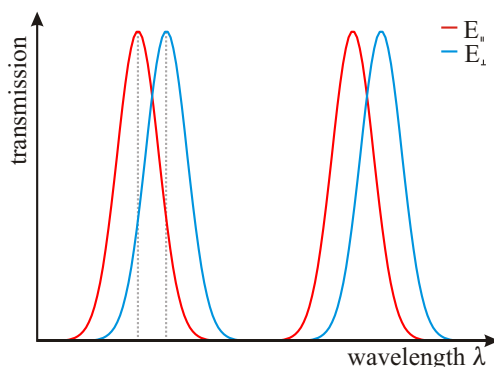


Figure 5.6: Off resonant transmission peaks of a cavity in V-configuration. E_{\perp} and E_{\parallel} have different transmissions when the cavity is not in resonance. The difference of these signals gives the dispersion shaped error signal.

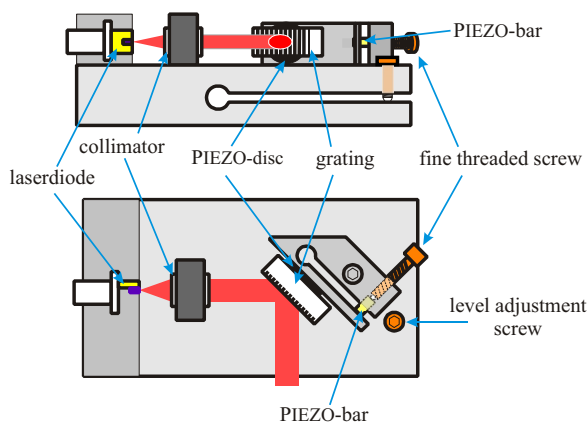
In resonance the two orthogonal linear polarizations (E_{\perp} and E_{\parallel}) of an incident beam will have the same phase, resulting in linear polarized light in transmission. Getting off resonance, the phase slope is different for both polarizations. If E_{\parallel} is lagging behind E_{\perp} on the high frequency side of resonance, it will be the other way around on the low frequency side (figure 5.6). This will add an circular component to the output beam. The analyzer of the adapted HÄNSCH-COULLAUD scheme remains exactly the same as in the original setup.

6 Generating the setup

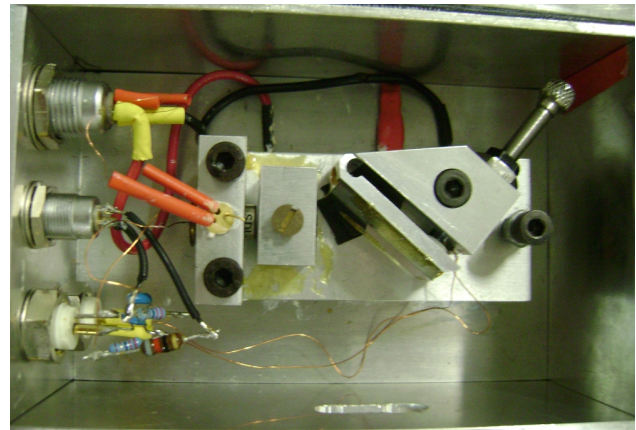
This section shows the generation of the experimental setup. We apply the theory we discussed above and point out difficulties and problems during the building procedure.

6.1 Diode laser

We start with a self locked laser diode build up in the LITTROW-configuration (figure 6.1) with a temperature control via PELTIER element. In LITTROW-configuration the minus first



(a) Animated [29].



(b) Real life.

Figure 6.1: Laserdiode with external grating in LITTROW configuration. The -1 diffractive order is reflected back into the laser and the 0 . order is coupled out.

order of diffraction is sent back into the laser and the zeroth order is coupled out. We can set the emitted wavelength by varying the angle of the grating. For the laser output being very sensitive to differences in temperature T , we have to control it. This is done by a PELTIER element as shown in figure 6.2.

This setup emits a very elliptical beam profile shown in figure 6.3a, as predicted in section 2.1. For better handling and fitting it is reasonable to correct the beam profile to a more

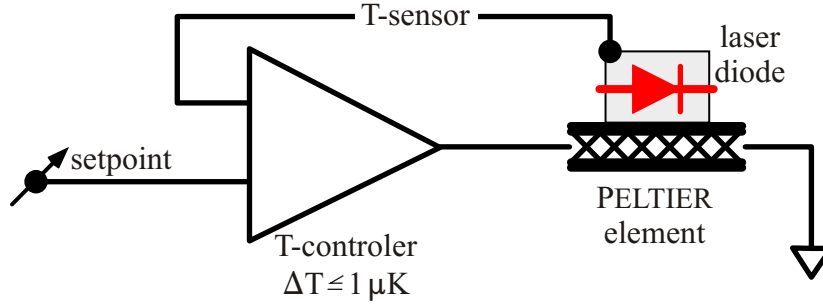


Figure 6.2: Temperature control of the laser via PELTIER element [29].

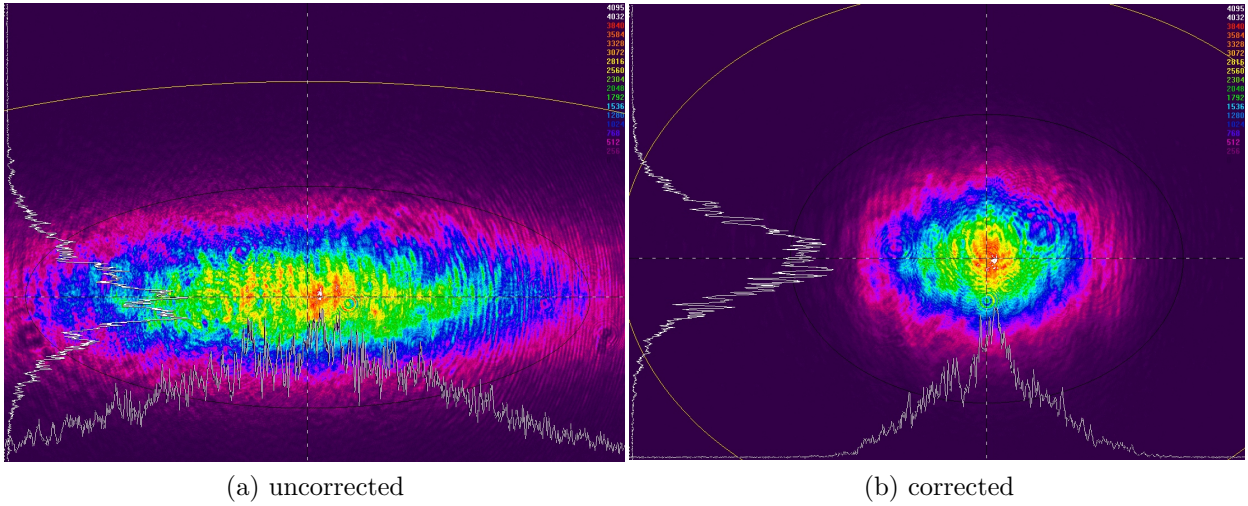


Figure 6.3: Beam profile of the laser output.

circle form (figure 6.3b). This can be done by using cylindrical lenses but we did it with an anamorphic pair of prisms for smaller path lengths. An anamorphic pair of prisms deflects the beam in one direction only as shown in figure 6.4.

To characterize the diode laser system we measure the characteristic diagram and gauge optical power versus injection current (figure 6.5). So we have a threshold current of (13.3 ± 0.5) mA. From this measurement we can calculate the quantum efficiency of the laser. This describes the efficiency the laser produces photons from the electrons. It is defined to be the electron rate r_{el} divided by the photon rate r_{ph} [13]:

$$\eta = \frac{r_{el}}{r_{ph}} = (0.64 \pm 0.12).$$

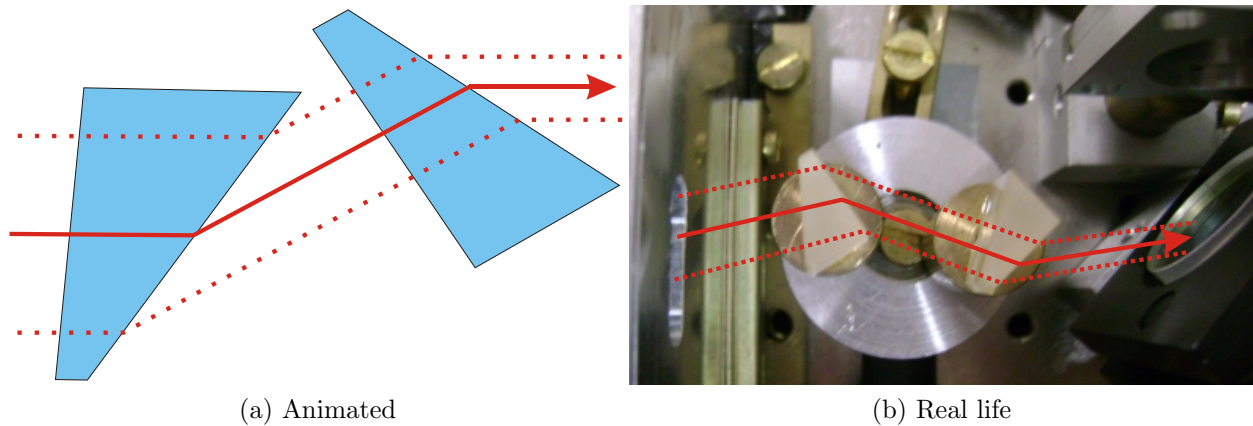


Figure 6.4: Elliptical beam cross sections can be converted to round cross sections using an anamorphic pair of prisms. Here deflection only occurs in one direction.

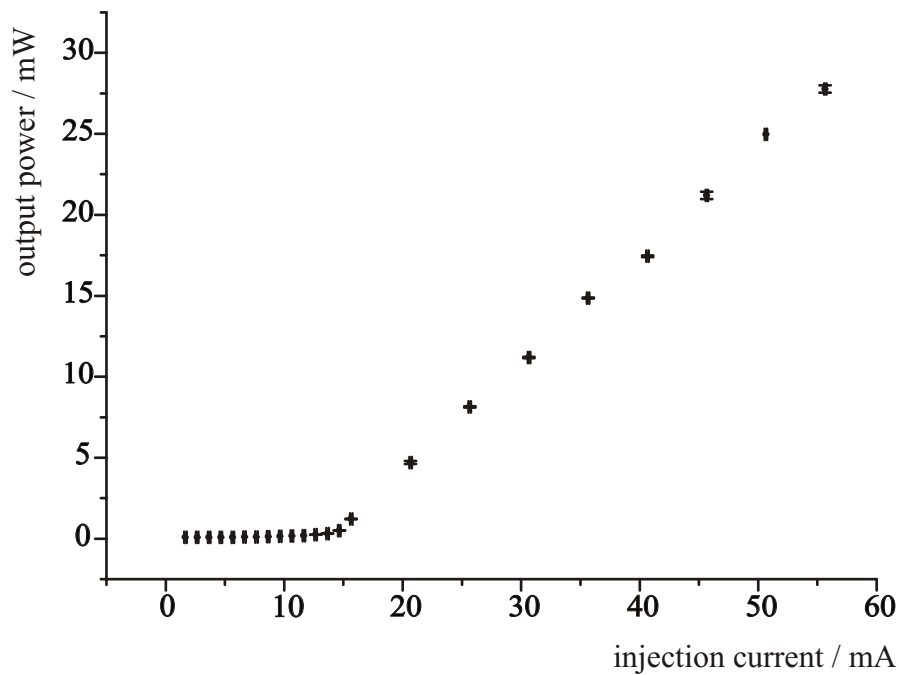


Figure 6.5: Threshold current of the laser system after optimizing the grating. The errors are the standard deviation from 10 measurements per point.

6.2 Building the cavity

In order to get an external feedback from a cavity we have to build one. We use home built cavities. These cavities have the quality characteristics and dimensions shown in figures 6.6 and 6.7. In order to put all parts together we start with the assembly of the lens side of



Figure 6.6: Components for building the cavity. From left to right: Pinhole, spacer, lens, spacer, mirror, brass screw thread, aluminum- e.g. zerodur rod, PIEZO tube, end cap.

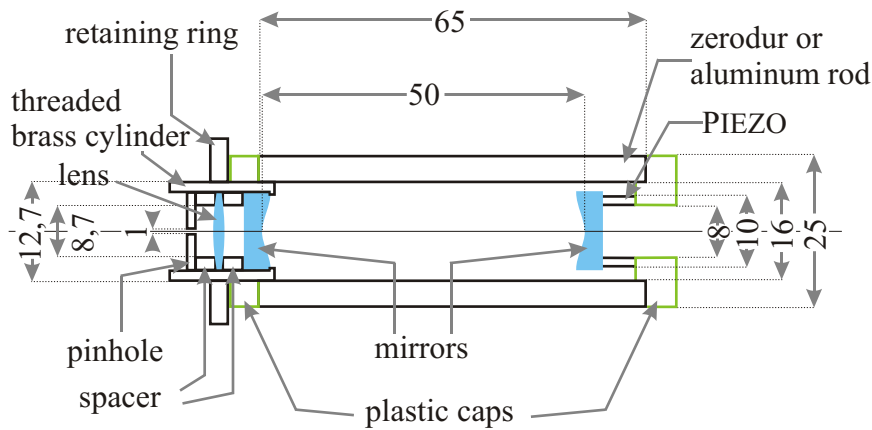


Figure 6.7: Detailed look on the cavity. All data is in millimeter. The curvature of the mirrors is 50 mm.

the cavity:

First the plastic cap with the thread has to be glued on the aluminum rod. It has to be made sure that the cap is glued exactly in the middle because the threaded brass cylinder has to fit in the aluminum rod as well and the tolerance is very low. Then the curved mirror has to be dropped into the threaded cylinder and fixed by screwing the spacer into the cylinder. Similarly the lens is fixed in the cylinder. The pinhole is optional.

Afterwards we assembly the PIEZO side of the cavity: We have to solder the cables on the inner and outer side of the PIEZO tube. Here we have to make sure that the inner electrode is positive and the outer electrode is the ground. The PIEZO fits in the end cap and has to be glued there. Through the feedthrough of the cap the outer cable has to be conducted out of the cavity. The inner cable can be conducted out directly through the laser port. Finally the end cap has to be glued on the aluminum rod. This cavity has the following properties:

- $\mathcal{F} := \frac{\Delta\nu_{\text{FSR}}}{\Delta\nu_{\text{cavity}}} = \frac{\pi\sqrt{R}}{1-R} \approx 250$
- $\Delta\nu_{\text{FSR}} = \frac{c}{4l} \approx 1,5 \text{ GHz}$
- $\Delta\nu_{\text{cavity}} = \frac{\Delta\nu_{\text{FSR}}}{\mathcal{F}} \approx 6 \text{ MHz}$

6.3 Building the fiberinterferometer

In order to fathom the starting point and to monitor our progress in narrowing the linewidth we have to build the self heterodyne scheme mentioned in section 3. At the beginning we used an already existing fiberinterferometer with a THORLABS BFL 48 fiber having a length of 200 m, an AOM at a frequency of 100 MHz, by courtesy of JULIAN and the group of PROF. DR. MARTIN WEITZ.

We were not able to actually measure something with this setup because we could not manage to get a beat signal on the photo diode. The reason most likely lies in the fiber being a multi mode fiber changing the incident mode to another. In order to solve this problem we had to build our own setup with a single mode fiber. The setup was generated mostly with parts available in the lab. Only the fiber and two fiber coupler had to be bought. We

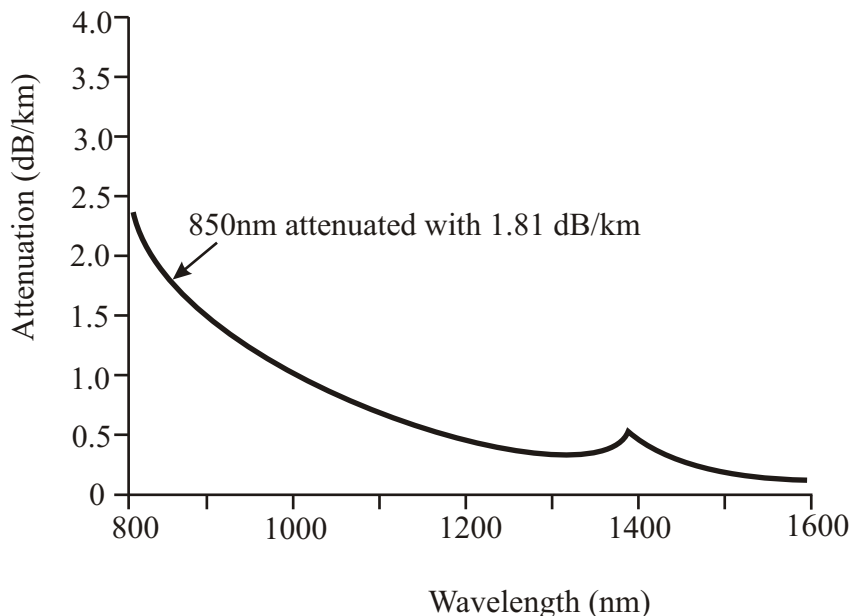


Figure 6.8: CORNING® SMF™-28 attenuation [26].

decided to buy a standard fiber from telecommunications: CORNING® SMF™-28 having the transmission properties shown in figure 6.8 and a length of 5 km. For the used wavelength

of 852 nm the transmission is 12.4 % at most.

For having the possibility to use the fiber interferometer to measure different lasers a SCHÄFTER and KIRCHHOFF fiber coupler is used to couple the laser light in. Then the laser light is split into two parts with a polarizing beam splitter (PBS). To control the intensity going into each arm we used a $\frac{\lambda}{2}$ wave plate in front of the PBS. The first arm is coupled into the fiber via two mirrors and a fiber coupler. The achieved transmission is 11.5%, which is a very good value for the theoretical value being 12.4 %. The second arm is feed through a $2f$ assembly with an AOM in the center. The lenses have a focal length of 10 cm and the AOM a modulation frequency of 324 MHz. The lens in front of the AOM focus the beam into the AOM. The second lens collimates the beam again. The reached diffraction efficiency of the AOM is 74 %. The zeroth order leaving the AOM is blocked by an iris, placed in a way that the first order beam penetrates the center of the iris.

Then both arms are combined again via four mirrors and a PBS. At this point we have to take care of both arms being heterodyne and having roughly the same intensity and spot size. This is necessary because the combined beams are reflected by one mirror through another, rotated PBS to project the heterodyne, orthographic beams to one plane of polarization to guarantee an interference. Then the recombined beam is focused on the photo diode. Both arms have a power of $(36 \pm 2)\mu\text{W}$.

The setup of the fiber interferometer is shown in figure 6.9.

6.4 The full setup

The full experimental setup consists of two parts: A stabilization part and an observation part. The stabilization part is the laser and the adapted version of the HÄNSCH-COULLAUD stabilization scheme. The observation part is the fiberinterferometer and a monitor cavity behind an optical isolator.

First we built the observation part. Doing so we first corrected the beam profile with an achromatic prism pair described in 6.1 and split the beam in two parts. Then we used two mirrors to walk the beam through the optical isolator. An optical isolator can be seen as an optical diode which allows the transmission of light in only one direction. It consists of a magnetic garnet crystal having the FARADAY effect, a permanent magnet and polarizing elements (figure 6.10). The two PBS have a 45° differential in the direction of their light transmission axes. There is a 45° FARADAY rotator interposed between the PBS. A forward light beam passing the optical isolator gets the following change:

Passing through the first PBS the light is split in two beams of linearly polarized light.

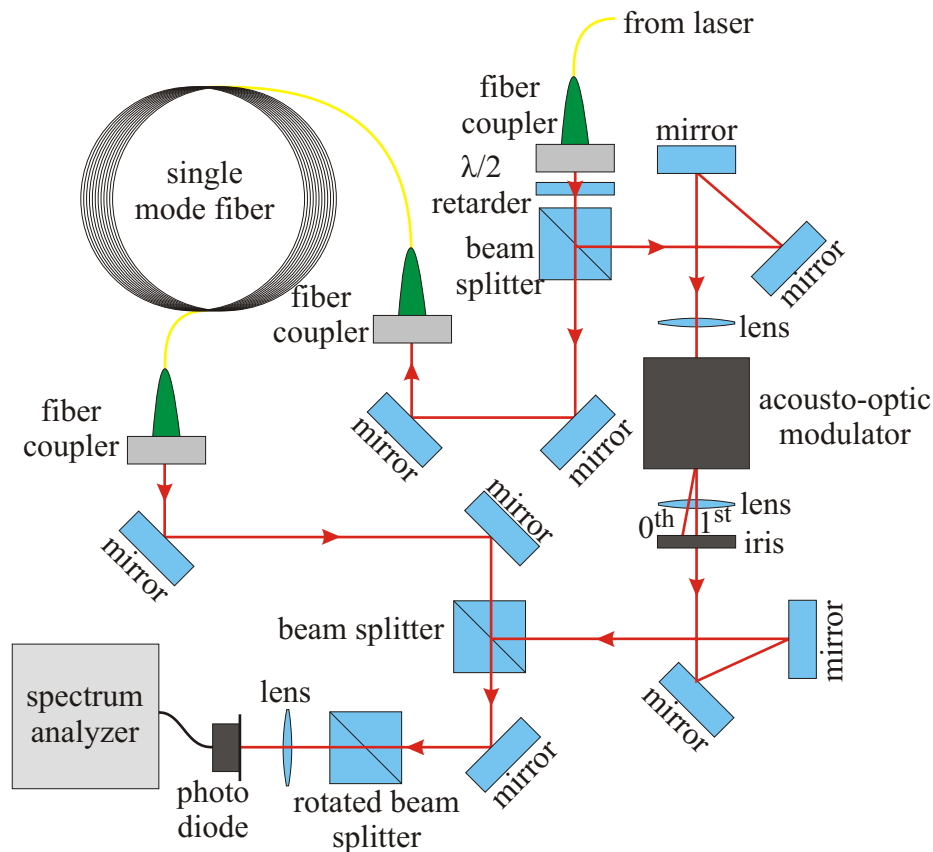


Figure 6.9: The fiber interferometer. Arm 1 is delayed by time by a fiber of 5 km length and arm 2 is frequency shifted by 324 MHz via an AOM.

One beam is blocked and the other passes through the FARADAY rotator, which rotates the direction of polarization about 45° . Then the light passes another PBS which is rotated about the same 45° in the direction of polarization was rotated before. Therefore the beam passes the second PBS without losses.

If the beam comes from the other direction to pass the optical isolator, the light is split into two beams of linear polarization by the rotated PBS. Passing through the FARADAY rotator, the plane of polarization is rotated by 45° in the same direction as the initial tilt. This light gets diverted completely into a beam dump by the second PBS.

To build the optical isolator in the setup we first have to maximize the throughput of the optical isolator. Then we have to turn the optical isolator around and minimize the signal. This procedure has to be repeated until the optimum is reached. To realize this we generated a very tight mount for the optical isolator. So we could turn the isolator without changing its position relatively to the laser beam (figure 6.11).

Since we now have the light through the optical isolator we do not get any feedback from

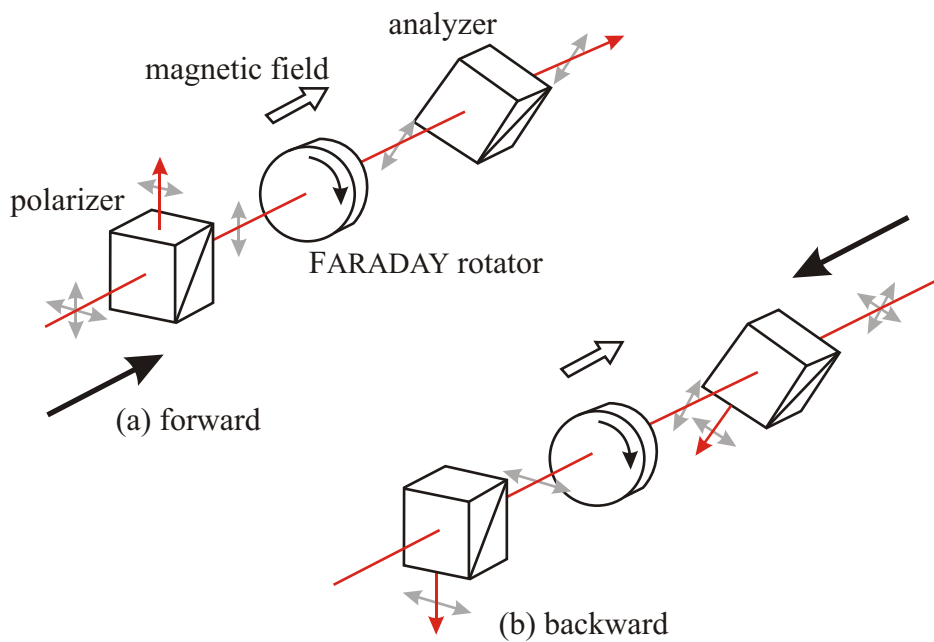


Figure 6.10: Structure of a polarization dependent optical isolator [28].

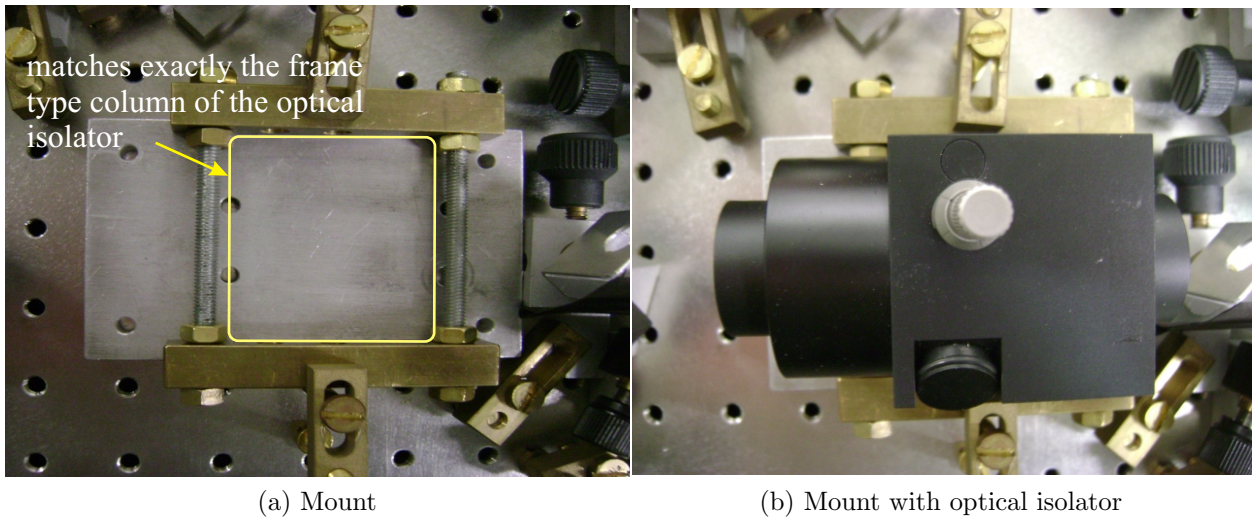


Figure 6.11: Self made mount to adjust the optical isolator. The optical isolator fits in very tightly and can be turned around without changing its position relatively to the laser beam.

the observation part. Right after the light is coming out of the optical isolator we split it again with a glass plate. The glass plate reflects 4 % of the incident light and transmits the rest. The smaller part of the light beam is used to monitor our signal with a reference cavity. So the light is guided into the reference cavity using two coupling mirrors in front of a lens.

The transmitted part of the glass plate is coupled into a short fiber via two mirrors to guide the beam to the fiber interferometer. A picture of the observation part is shown in figure 6.12.

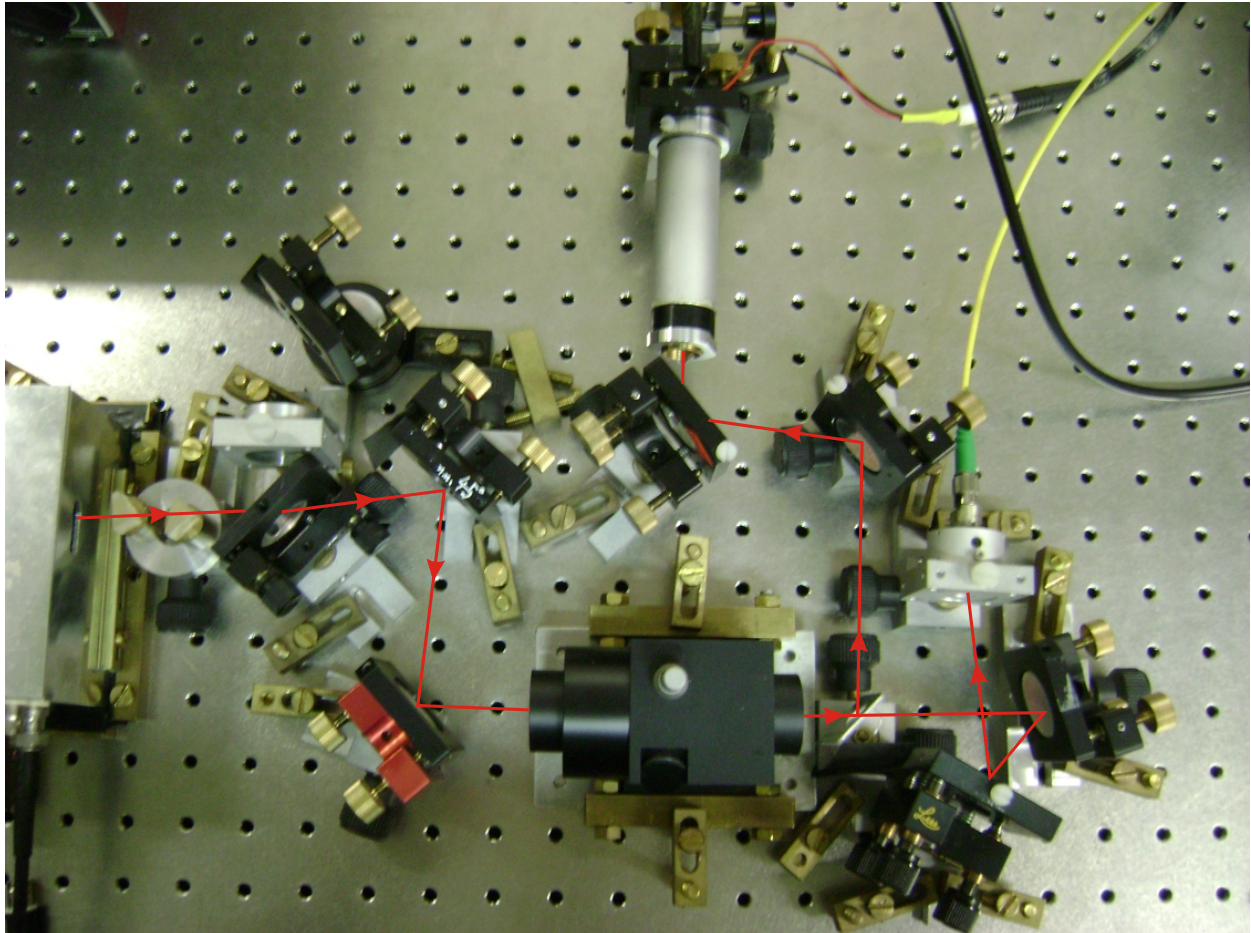


Figure 6.12: Observation part of the setup.

To couple the laser light into the monitor cavity it is useful to use an iris. We aligned the mirrors such that the laser beam is incident at the center of the cavity mirror, and also such that the cavity reflection hits the coupling mirrors at the same spot as the input laser beam. We then can observe the reflection from the cavity on the iris: If the beam size is roughly the same as the input laser beam at the iris, then the input wavefront curvature is well chosen. If not we either have to correct the radius of curvature or the position of the waist is not near enough to the waist of the cavity. Moving the lens will solve this problem. After both beams having the same size we look at the cavity transmission with a photo diode placed behind the cavity, while sweeping the laser frequency. Once modes are observed we adjust the sweep so that about two free spectral ranges are covered. A problem arises to figure out

which peak actually corresponds to the TEM_{00} mode. To solve this we can close the iris to a small size. This attenuates the coupling to higher modes more than to the TEM_{00} mode because it is the smallest mode. With some patience the TEM_{00} mode will couple to the cavity.

The stabilization part is shown in figure 6.13. Here we used the adapted HÄNSCH-COULLAUD stabilization technique described in section 5.2. To couple the type I beam

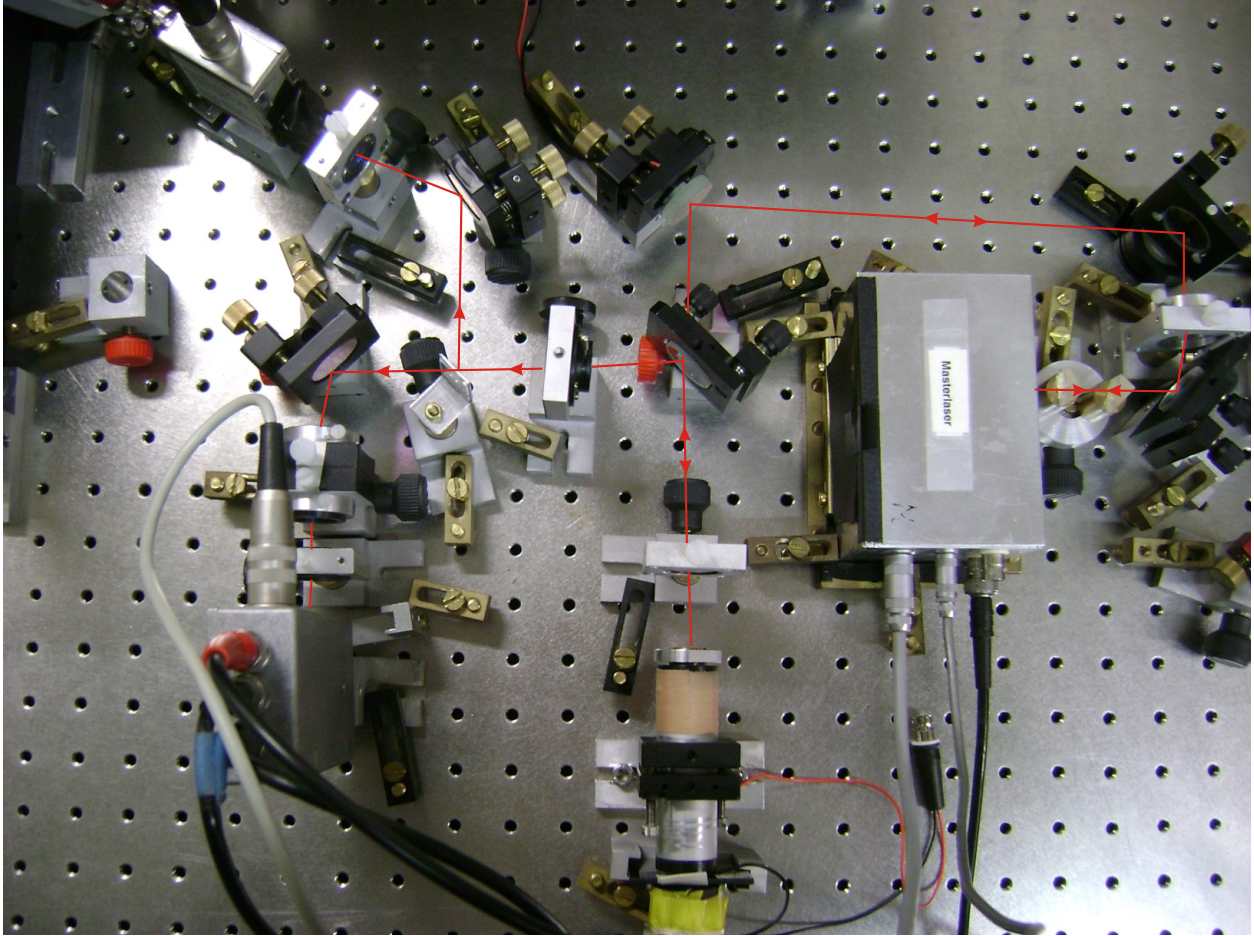


Figure 6.13: Stabilization part of the setup.

out after being in the cavity the irradiation is through a substrate. The substrate acts like a glass plate and allows to send the type I beam to the HÄNSCH-COULLAUD analyzing scheme. In order to get an acceptable error signal the coupling to the cavity has to be very good. The theoretical and practical aspects of coupling light into the cavity have been discussed above. To realize the coupling to this cavity in reality we have to think about a method to avoid feedback from the cavity to the laser, but align the cavity in a way that feedback is possible. We want to avoid feedback during adjustment because the transmission signal

from the cavity is destroyed by the instable feedback. In short: We do not want feedback for adjustment but afterwards. We came up with the following solution: Build in an optical isolator in a way that the light can couple to the cavity but not back to the laser and remove the optical isolator after adjustment. Unfortunately this idea did not work. The coupling to the cavity was going well but after removing the optical isolator the coupling was disturbed. The optical isolator must somehow shift the optical path in the plane perpendicular to the table and beam that the coupling after removing the optical isolator is not good enough. The vital idea was to exchange the substrate carefully with a high reflective mirror. The substrate and the mirror are equal in size and shape and can be exchanged in a fixed mirror mount without effecting the beam path. Due to the high reflective mirror the intensity irradiated into the cavity is very low since most of the incident light is reflected into a beam dump. Therefore the transmitted light of the cavity has even lower intensity and only a very tiny part is heading back to the laser. This tiny part can be blocked with an attenuator. So we can couple the light to the cavity without getting feedback. After coupling the light to the cavity, following the rules explained above, the mirror is replaced by the substrate again and the attenuator is removed and the laser gets feedback. To stabilize the laser the transmitted type I beam is coupled out to the HÄNSCH-COULLAUD analyzing scheme.

7 Results

The error signal provided by the HÄNSCH-COULLAUD stabilization setup is shown in figure 7.1. The signal is generated by scanning the grating of the LITTROW configuration. This

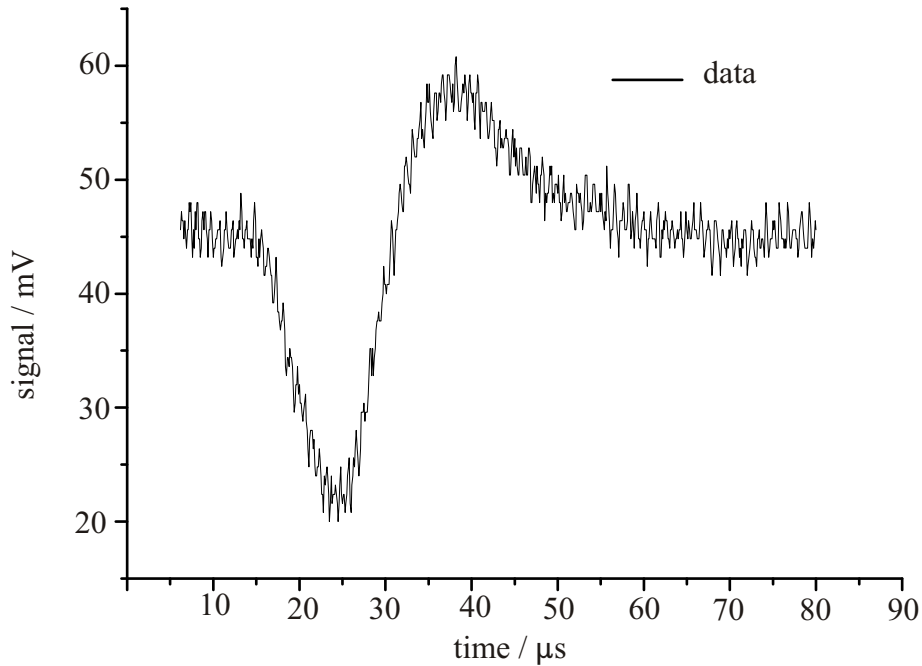


Figure 7.1: Measurement of the error signal of the HÄNSCH-COULLAUD stabilization technique.

changes the frequency of the laser output and we get two different resonances for the two polarizations. The differential amplifier gives the shown data. We can see that it looks like predicted in section 5.1. The slight asymmetry can be explained by having a better cavity transmission for one linear polarization than for the other. This can be due to a minimal misalignment of the mirrors during the gluing process described in section 6.2. Never the less we can lock to the signal.

The locking is done with a lock box to the zero crossing of the dispersive signal. Here is no phase shift between the two directions of polarization and the cavity is in resonance. If there is a detuning to the left or the right of the zero crossing the voltage will fall or rise respectively. One of the mirrors for coupling the light into the cavity is mounted on a PIEZZO crystal. This crystal is triggered by the lock box which therefore can variate the path length of the beam heading towards the cavity. Changing the path length, changes the incident phase as well. So the lock box can control the relative phase shift to be zero.

The beat signal of the LITTROW configuration is shown in figure 7.2. The FWHM of the signal is $(5,26 \pm 1,82)$ MHz corresponding to a laser linewidth of (2.63 ± 0.91) MHz using equation (3.1). The FWHM is taken on a linear scale which is not plotted for lack of space. This measurement confirms our measured values via a transmission spectrometric procedure, described in the diploma thesis of JULIA KEMP.

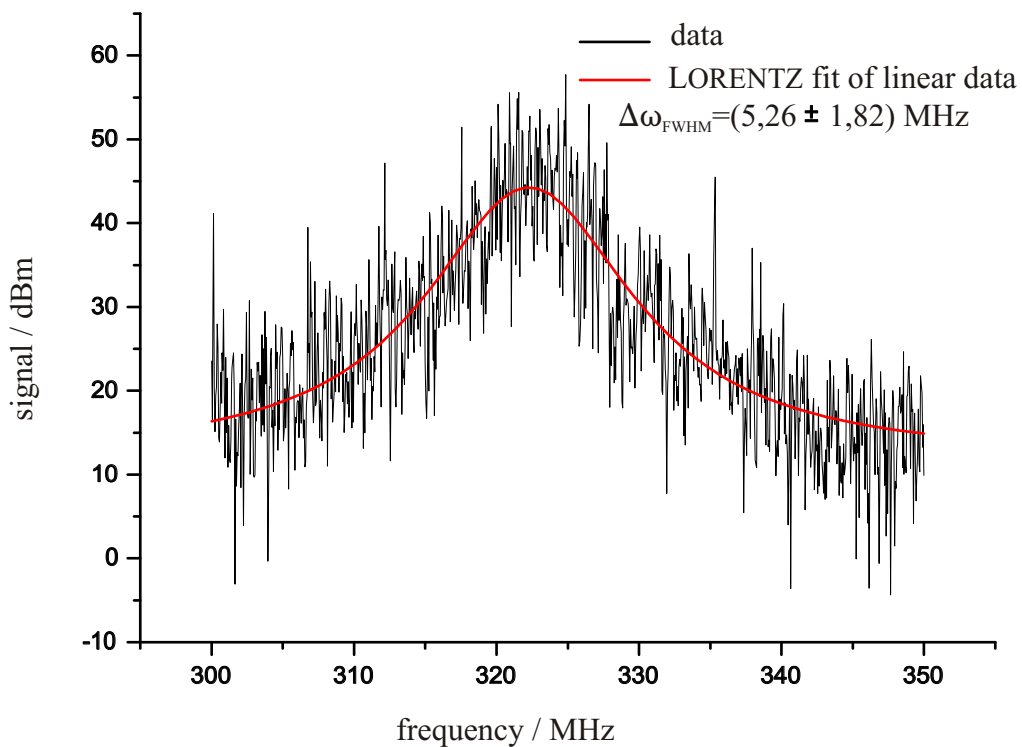


Figure 7.2: Measurement of the laser linewidth in LITTROW configuration without getting feedback from the cavity. Sweep time is 1 ms, RBW=VBW= 0.47 MHz.

Figure 7.3 shows the beat signal of the stabilized laser. As expected the FWHM of this beat signal is much thinner. It is (0.55 ± 0.34) MHz with a corresponding laser linewidth of (0.275 ± 0.170) MHz. This FWHM is taken on a linear scale also.

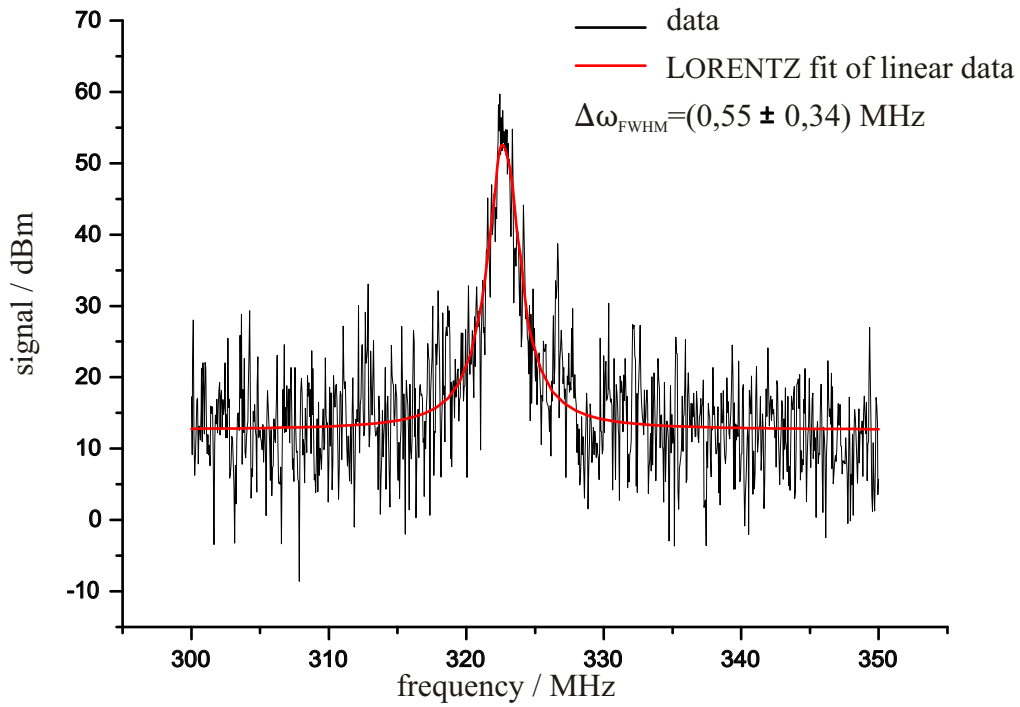


Figure 7.3: Measurement of the laser linewidth getting feedback from the cavity. Sweep time is 1 ms, RBW=VBW= 0.47 MHz.

Since the actual locking laser of the CQED experiment has a linewidth of about 10 kHz there has to be an improvement of the linewidth achieved in this result. Some possibilities to improve the setup are made in the next chapter.

8 Conclusion and outlook

The setup generated in this diploma thesis supplies first promising results in order to generate a compact long term frequency stabilized diode laser system. In addition to the presented setup we studied a similar system with a plane-parallel cavity described in detail in the diploma thesis of JULIA KEMP. This setup provided dissatisfactory results which led us to concentrate our efforts to the V -configuration.

Beginning with a linewidth of (5.26 ± 1.82) MHz it was possible to reduce it by a factor of 10 to (0.55 ± 0.34) MHz. Many problems in generating the setup have been solved and described as well. The actual locking laser of the CQED experiment has a linewidth of about 10 kHz. So this setup has to be improved to achieve comparable results.

A first step in further narrowing the linewidth is to make the setup more compact and stable. This could be done by building it into a special made full metal jacket. Here the whole setup should be on one solid block of metal with drilled holes for the light passing through. This would improve the resistance and stability of the system against vibrational and thermal changes of the environment and can be realized by the mechanical workshop. Then the feedback from the LITROW configuration has to be removed so that there is the optical feedback from the cavity only. This should on the one hand improve the stability of the lock because there is no need to have two cavities to be resonant at the same time but on the other hand complicate the selection of the wavelength.

A fancy way to stabilize and miniaturize the setup is to build it completely in fiber. This means taking a pigtailed laser diode, use fiber beam splitter and pigtailed photo diodes. These parts are available from different companies in different versions. The critical part is a fiber based cavity. A very impressive way to build a fiber cavity is realized by J. REICHEL and T. W. HÄNSCH *et al* in 2010 [17]. Here a fiber based FABRY-PEROT cavity with CO_2 laser machined mirrors combines very small size and high finesse $\mathcal{F} \geq 130.000$. Furthermore this cavity has a small waist and mode volume and good mode matching properties between the fiber and cavity modes. The proposed design of the cavity cannot be used for this experiment, because we want the cavity to operate in V configuration for getting feedback in resonance only. To adapt the design to run in V configuration a theoretical possible solution

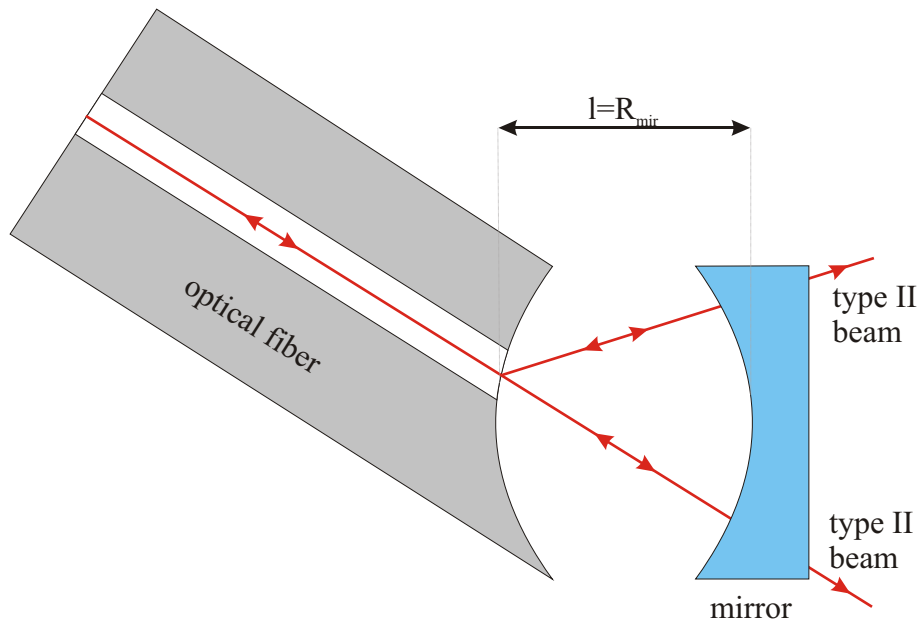


Figure 8.1: Sketch of a cavity with one mirror being a coated spherical end of an optical fiber.

is to machine the mirror on the end of the fiber under an angle that allows V configuration. This is shown in figure 8.1. In this alignment the error signal for the adapted HÄNSCH-COULLAUD stabilization scheme can be taken from the transmitted type II beams. It has to be determined if this adaption to the fiber cavity can be realized.

For the linewidth of the existing setup being in the region of 100 MHz and the resolution of the fiberinterferometer being 40 kHz the fiber should be replaced with a longer one.

We conclude that the generated setup supplies first promising results, but has to be improved further on to actually replace the existing locking laser.

A Appendix

A.1 Anti reflex coating

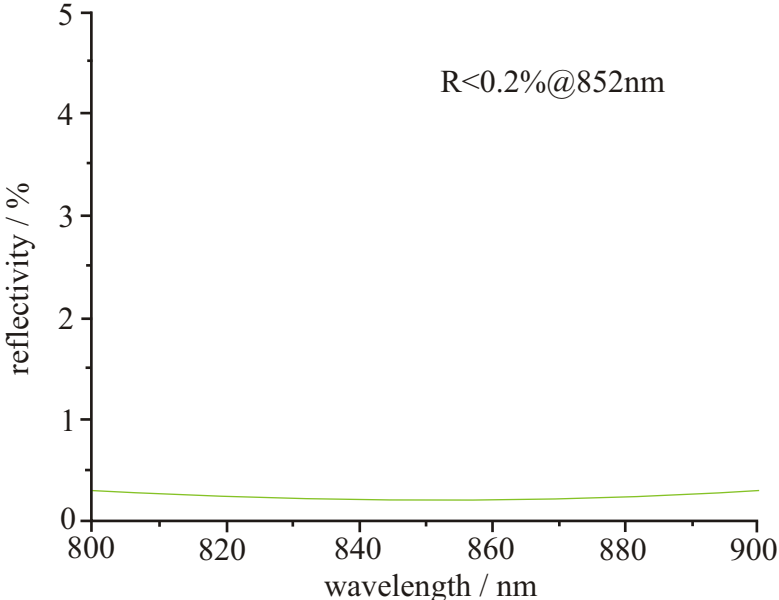


Figure A.1: Properties of the anti reflex coating of the company BEFORT WETZLAR. The reflectivity of a wavelength of 852nm is less than 0.2%.

Bibliography

- [1] G.D BOYD and H. KOGELNIK, '*Generalized confocal resonator theory*',
BELL sys. Tech. J., vol. 41, pp. 1347-1369 (July 1962)
- [2] I.N BRONSTEIN *et al*, '*Taschenbuch der Mathematik*',
Verlag HARRI DEUTSCH (2001)
- [3] B. DAHMANI, L. HOLLBERG and R. DRULLINGER, '*Frequency stabilization of semi-conductor lasers by resonant optical feedback*',
Opt. Lett. 12, 876 - 878 (1987)
- [4] R.W. FOX, C.W. OATES and L.W. HOLLBERG, '*Stabilizing Diode Lasers To High-Finesse Cavities*', Experimental Methods in the Physical Sciences Volume 40, Pages 1-46 (2003)
- [5] C.H. HENRY, R.A. LOGAN and F.R. MERRIT, '*Measurement of gain and absorption spectra in AlGaAs buried heterostructure lasers*',
J. App. Phys., vol. 51, p. 3042 (1980)
- [6] C.H. HENRY, R.A. LOGAN and K.A. BERTNESS, '*Spectral dependence of the change in refractive index due to carrier injection in GaAs lasers*',
J. Appl. Phys., vol. 52, pp. 4451-4461 (1981)
- [7] C. H. HENRY, '*Theory of the linewidth of semiconductor lasers*',
IEEE J. Quantum Electron. 18, 259-264 (1982)
- [8] T. W. HÄNSCH and B. COUILLAUD, '*Laser Frequency Stabilization By Polarization Spectroscopy Of A Reflecting Reference Cavity*',
Optics Communications, Vol. 35, No. 3, pp. 441-444 (1980)
- [9] H. KOGELNIK, '*Imaging of optical mode - Resonators with optical lenses*',
BELL sys. Tech. J., vol. 44, pp. 455-494 (March 1965)
- [10] H. KOGELNIK and T. LI, '*Laser Beams and Resonators*',
Applied Optics, Vol. 5, No. 10, p. 1550-1567 (October 1966)

-
- [11] L.D. LANDAU and E.M. LIFSHITZ, '*Electrodynamics of Continuous Media*', Reading, MA: ADDISON-WESLEY sect.63. (1960)
- [12] M. LAX, '*Classical noise V. Noise in self-sustained oscillators*', Phys. Rev. 160, p. 290 (1967)
- [13] D. MESCHEDE, '*Optik, Licht und Laser*', 2. Auflage Teubner Verlag, Wiesbaden (2005)
- [14] J. VON NEUMANN, '*Notes on the Photon-Disequilibrium-Amplification Scheme*' (1953), IEEE J. Quantum Electron. 23, 659 (1987)
- [15] OKOSHI et al., '*Novel method for high resolution measurement of laser output spectrum*', Electronics Letters Vol. 16, No. 16 (1980)
- [16] J. R. PIERCE, '*Theory and Design of Electron Beams*', New York: VAN NOSTRAND, p. 194 (1954)
- [17] J. REICHEL and T.W. HÄNSCH *et al*, '*A fiber FABRY-PEROT cavity with high finesse*', *New Journal of Physics* **12** (2010) 065038 (23pp)
- [18] L. E. RICHTER, '*Linewidth Determination from Self-Heterodyne Measurements with subcoherence Delay times*', IEEE J. Quantum Electron. 22, 2070-2074 (1986)
- [19] F. RIEHLE, '*Frequency Standards - Basics and Applications*', Wiley-VCH, Weinheim (2004)
- [20] A. L. SCHAWLOW and C. H. TOWNES, '*Infrared and Optical Masers*', Phys. Rev. 112, 1940-1949 (1958)
- [21] A. E. SIEGMAN, '*Lasers*', *University Science Books*, Sausalito (1986)
- [22] P. A. TIPLER, '*Physik*', *Spektrum Akademischer Verlag*, Berlin, Oxford third edition (1998)
- [23] J.T. VERDEYEN, '*Laser electronics*', PRENTICE-HALL Inc. (1986)
- [24] A.YARIV, P.YEH, '*Photonics: Optical Electronics in Modern Communications*', Oxford University Press (1958)

From the internet

- [25] <http://dict.leo.org/ende?lang=de&lp=ende> (March 10, 2011)
- [26] CORNING[®], '*SMFTM-28 product information*',
<http://www.corning.com> (June 08, 2010)
- [27] <http://www.datasheetarchive.com/pdf/Datasheet-036/DSA0019992.pdf>
(March 08, 2011)
- [28] <http://www.fdk.co.jp/laboratory/hikariaai-e.html> (February 23, 2011)
- [29] <http://www.iap.uni-bonn.de/o11> (February 12,2011)
- [30] http://www.rp-photonics.com/semiconductor_lasers.html (February 06, 2011)

Affirmation

I stand here with that I have written this diploma thesis independently and have used no other than the specified sources and tools. All areas of this diploma thesis that are literally or in substance taken from other sources were identified as such.

Bonn, March 10, 2011

Signature